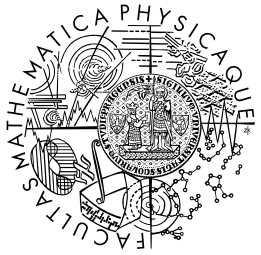

FACULTY
OF MATHEMATICS
AND PHYSICS
Charles University

DOCTORAL THESIS

Petr Fatka

Identification methods of genetically related asteroids

Astronomical Institute of Charles University

Supervisor of the doctoral thesis: Mgr. Petr Pravec, Ph.D.
Study programme: Theoretical Physics, Astronomy and Astrophysics
Study branch: P4F1

Prague 2020

I declare that I carried out this doctoral thesis independently, and only with the cited sources, literature and other professional sources.

I understand that my work relates to the rights and obligations under the Act No. 121/2000 Sb., the Copyright Act, as amended, in particular the fact that the Charles University has the right to conclude a license agreement on the use of this work as a school work pursuant to Section 60 subsection 1 of the Copyright Act.

In Prague, January 21, 2020 .....

First of all, I would like to thank my supervisor Petr Pravec for his guidance, his advice and all of the time he reserved for me. I also thank David Vokrouhlický for his suggestions during our many consultations. Velké díky patří celé mé rodině za jejich nekonečnou podporu a časté povzbuzovaní. Obzvláště děkuji svým rodičům bez jejichž podpory by bylo vše o mnoho težší.

Title: Identification methods of genetically related asteroids

Author: Petr Fatka

Institute: Astronomical Institute of Charles University

Supervisor: Mgr. Petr Pravec, Ph.D., Astronomical Institute of the Czech Academy of Sciences

Abstract: In this thesis, I describe the main ideas and summarize the results of four refereed papers I contributed to (three times as the second author and once as the first author). The first step of each of these papers was the identification of genetically related asteroid and their membership confirmation. Since members of asteroid pairs and clusters have a very similar heliocentric orbits, we employed and further developed methods based on backward orbital integrations. The chronologically first paper (Pravec et al., 2018) deals with asteroid clusters and their similarity to asteroid pairs. The second paper (Pravec et al., 2019) is a complex study of 93 asteroid pairs with many interesting results, such as the existence of binary asteroids among asteroid pairs. The third paper (Moskovitz et al., 2019) deals with an identification of asteroid pairs in the near-Earth population and a detail study of two probable asteroid pairs. The fourth paper, Fatka et al. (2020), studies the phenomenon of cascade disruption in asteroid clusters, which results in multiple generations (with different ages) of escaped secondaries in some asteroid clusters.

Keywords: asteroids, asteroid pairs and clusters, backward integrations

Contents

Introduction

The existence of asteroid pairs on highly similar heliocentric orbits in the Main Asteroid Belt was first discovered by Vokrouhlický and Nesvorný (2008). They showed that it is very unlikely for these pairs to be on such similar orbits only by chance and they proposed that the 60 studied pairs were genetically related and come from a single parent asteroid. Later, Pravec and Vokrouhlický (2009) enhanced the identification method of asteroid pairs by taking a statistical approach, which helped to quantify the statistical significance of each pair with respect to their surrounding. In total, 73 significant pairs were found and for most of them a backward orbital integration was performed to further support the theory of a common origin. Scheeres (2007) introduced a scenario of a possible formation mechanism of these pairs, which assumed a rotational fission of a rubble pile asteroid followed by an escape of the smaller component ("secondary"). Pravec et al. (2010) created a model based on the fission scenario introduced by Scheeres (2007) and checked its predictions with a sample of 32 asteroid pairs. They found a strong correlation between the rotational period of the larger component ("primary") and the mass ratio of the escaped secondary and the primary. The common origin for many of the asteroid pairs has been also supported by the similar photometric colors and/or spectral properties of the two components.

Apart from the old asteroid families that were created $10^7 - 10^9$ years ago by catastrophic collisions of asteroids and the very young (with typical age $< 10^6$ years) asteroid pairs in the Main Belt, there also exist small groups of asteroids on similar heliocentric orbits. Nesvorný et al. (2006) and Nesvorný and Vokrouhlický (2006) identified first four of these clusters. Pravec and Vokrouhlický (2009) discovered another five of these clusters. A few other discoveries was made later, e.g., by taking a different approach Novaković et al. (2014) discovered an interesting asteroid cluster with one member being an active asteroid. These clusters are suspiciously similar to the asteroid pairs, their heliocentric orbits are also very similar, their age is within a few million years and backward orbital integrations suggest small separation velocities (at least for some of them).

In this work, we performed a further study of asteroid pairs and clusters. In Pravec et al. (2018), we studied 13 asteroid clusters, including 3 new that we discovered. We performed an orbital analysis of 11 clusters (for two clusters the analysis was performed shortly before our paper). Among other, we also confirmed that the correlation of primary's rotational period and the mass ratio between the primary and all escaped secondaries is also valid for asteroid clusters suggesting a formation by a rotational fission. My contribution in this paper was the execution of the backward orbital integrations and the age estimation for the members of each cluster. I was also involved in the search for new cluster members and their membership verification. In Pravec et al. (2019), we performed a complex study of 93 asteroid pairs and as a by-product, we discovered 3 new asteroid clusters. In this paper I was responsible for the confirmation that studied pairs are in fact pairs and not clusters, the backward orbital integrations and estimation of the ages of studied pairs, taxonomy assignment from the `Sloan Digital Sky Survey` for asteroids and I also performed photometric observations for some of the asteroids. In Moskovitz et al. (2019), we studied the existence of

asteroid pairs in the near-Earth population and performed a detailed study for two candidate pairs. I contributed by testing various metrics for orbital similarity description and subsequent search for asteroid pairs and also by performing the backward orbital integrations and their analysis. In Fatka et al. (2020), we explored the phenomenon of the existence of asteroid clusters with at least two generations of secondaries (caused by two disruption events). I was responsible for the search of such clusters, the backward orbital integrations leading to pair age estimation and for constructing a simple model testing a possibility of two rotational fission events caused by the Yarkovsky–O'Keefe–Radzievski–Paddack effect.

During my PhD studies I performed number of photometrical observations with several telescopes from a few observatories. A short summary follows.

- 1.54-m telescope (Danish Telescope) at the LaSilla Observatory, Chille, 173 nights (13 locally, 160 remotely observed) in years from 2016 to 2020
- 0.65-m telescope (Mayer's Telescope) at the Ondřejov Observatory, Czech Republic, 22 nights (all locally observed) during the years 2017 and 2019
- 1.8-m (Perkin's Telescope) and 1.1-m (Hall's Telescope) telescopes at the Lowell Observatory, Flagstaff, Arizona, USA, a total of 22 nights (all locally observed) during September and October 2017
- 1.5-m (AZT-22) and 1-m (Zeiss-1000) telescopes at the Maidanak Observatory, Uzbekistan, a total of 13 nights (all locally observed) in September 2018
- 1.6-m (KMTNet SAAO) telescope at the South African Astronomical Observatory, Sutherland, South Africa, 2 nights (all locally observed) during September 2019

1. Asteroids in our Solar System

In this chapter, we will cover the basic information about asteroids. We will briefly mention asteroid distribution across the Solar System, asteroids basic properties, orbit description, two non-gravitational effects acting on asteroids and a possible disruption mechanism leading to the formation of asteroid pairs and clusters. This text is not intended as an educational material, but only as a brief revision provided for readers who are already familiar with these topics. For a more complete information about given topics, we refer interested readers to the references mentioned in given sections.

1.1 General properties of asteroids

Asteroids are small, rocky objects orbiting around the Sun. The first discovered asteroid[1] was Ceres observed by Guiseppe Piazii on 1 January 1801 (Piazzi, 1802). Since then, over 930 000 objects in our Solar System are currently classified as asteroids, with the number still rapidly growing mainly due to several running sky-surveys.

1.1.1 Asteroid distribution in our Solar System

Asteroids are the most abundant objects in the Solar system, that holds together by their own gravity, and can be found almost everywhere. But the vast majority of known asteroids (about 90%) is located in the Main Asteroid Belt reaching from 2.1 to 3.5 AU and inclinations up to 20°. According to `JPL Small-Body Database`[2], there is currently (January 2020) almost 22 000 known near-Earth asteroids, which is about 2.3% of the whole known asteroid population. Next abundant group of asteroids are Jupiter's Trojans (7 756 members as of January 2020) orbiting at similar orbits as Jupiter ($\sim$ 5.2 AU) near Lagrange points L_4 and L_5. We also know about 500 asteroids orbiting between the orbits of Jupiter and Neptune, which are called Centaurs. Objects orbiting beyond the orbit of Neptune are called trans-Neptunian objects (TNOs for short) and about 3 200 of them have been discovered. However, it should be noted that the number of discovered asteroids is strongly biased and does not represent the true distribution of asteroids. Figure 1.1 shows that in fact the population of TNOs is the most abundant group of asteroids, at least regarding large asteroids. All of these (and the not mentioned) asteroid groups are very interesting and deserve a study of their own, however, in the scope of this work, we will focus mainly on the largest group of asteroids - the Main Asteroid Belt with a small detour to the near-Earth asteroid population.

[1] Ceres was originally classified as a planet and it was reclassified as an asteroid later in 1863. In 2006 Ceres was reclassified again and is now considered to be a dwarf planet (taken from https://solarsystem.nasa.gov/planets/dwarf-planets/ceres/exploration/ on 11.1. 2020).

[2] Available at "https://ssd.jpl.nasa.gov/".

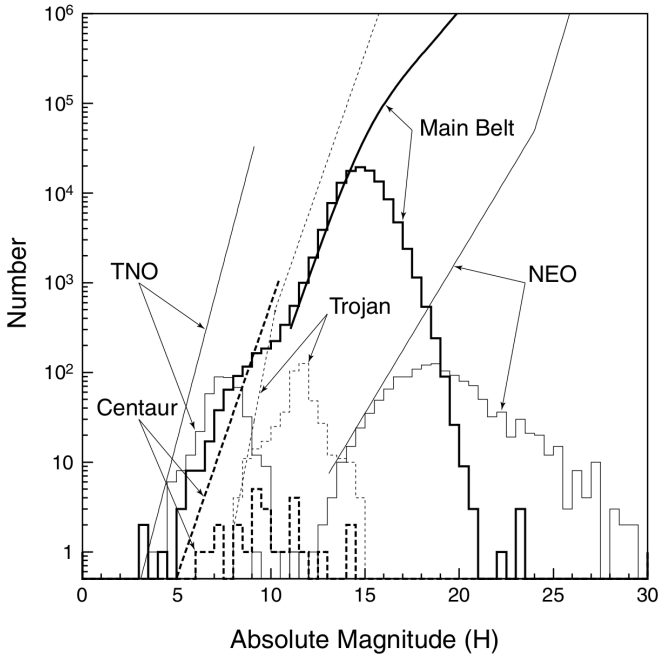

Figure 1.1: Comparison of the bias-corrected H distribution of asteroids and the observed H distribution (as of July 18, 2001) for five groups of asteroids (Jedicke et al., 2002).

The Main Asteroid Belt

The distribution of asteroids in the Main Belt is not uniform (see Figure 1.2), but it is influenced by several factors. One of them comes from the presence of large planets, especially Jupiter, and leads to unstable-orbits regions, named Kirkwood gaps after Daniel Kirkwood, who noticed them first in the second half of the 19th century. The cause of some of these gaps are resonances in the mean motion with Jupiter, such as resonance 3:1 (asteroid's orbital period is 3× shorter than Jupiter's) located at distance 2.50 AU from the Sun, 5:2 at 2.82 AU or 7:3 at 2.96 AU. Also three-body mean-motion resonances, such as, 5:2:2 with Jupiter:Saturn:asteroid, located at 3.175 AU, influence asteroid's orbit. Even though about 14% of asteroids are located in the three-body resonances (Smirnov et al., 2018), the field of action of the 3-body resonances is typically much smaller and they do not influence the distribution of asteroids as strongly as the two-body resonances. Another type of resonances, called secular resonances, disturb asteroid orbit when its precession rate of the argument of the periapses (ω) or the longitude of the ascending nodes (Ω) is a ratio of small integers with a planet's precision rate of ω or Ω. An example of this type of resonance is a ν_6 resonance with Saturn.

Near-Earth asteroids

Asteroids, whose perihelion distance is < 1.3 AU or whose aphelion distance is > 0.983 AU are classified as near-Earth asteroids (Morbidelli et al., 2002). Their orbital distribution is shown in Figure 1.3 and it is notable that there is not as many features as in the Main Belt. Since every heliocentric orbit in the proximity to the Earth becomes chaotic sooner or later (with few exceptions, such as

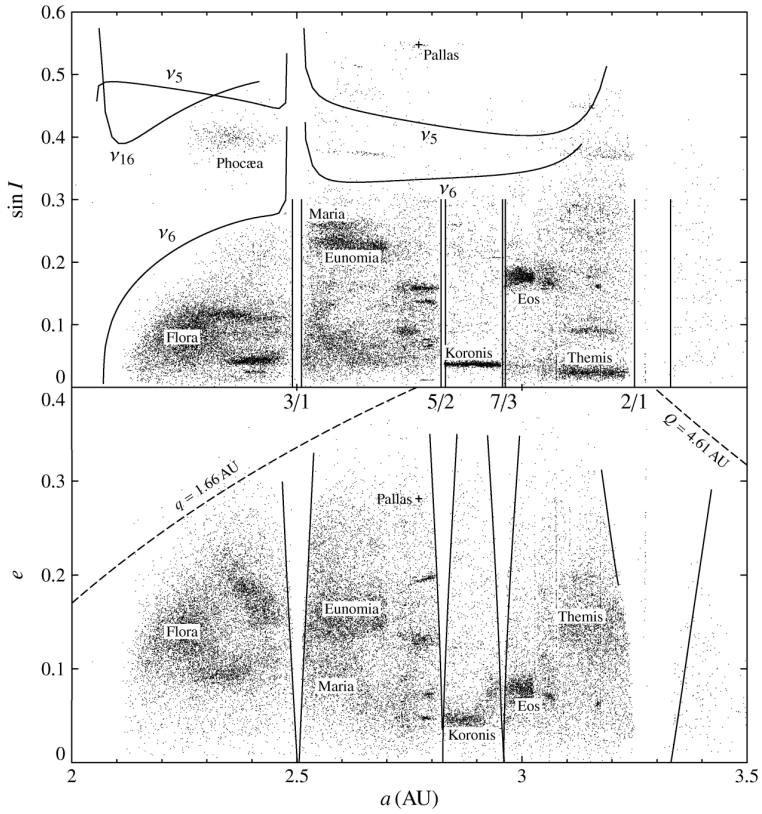

Figure 1.2: Orbital distribution of Main Belt asteroids in proper orbital elements (see Section 1.2.3 for explanation of the proper orbital elements) with labels of a few asteroid families. Solid lines denote borders of orbital resonances, while the dashed lines denotes proximity to the orbit of Mars ($q \doteq 1.66$) or Jupiter ($Q \doteq 4.61AU$). Figure taken from Bertotti et al. (2003)

1:1 mean motion resonance), there must be a constant source of new near-Earth asteroids, otherwise we would not find any at this time anymore. A significant fraction of the near-Earth population comes from large catastrophic collisions in the Main Belt that happened several million years ago. Fragments of collided asteroids could be ejected directly to large eccentricity orbits, making their aphelion distance < 1.3 AU. Other sources of near-Earth asteroids are resonances in the Main-Belt, especially the secular ν_6 resonance and mean motion resonances 3:1, 5:2, and 2:1 with Jupiter. Asteroid can enter into these resonances due to the Yarkovsky effect (see Section 1.3.1). About 6% of the near-Earth population comes from the Jupiter-family comets population.

In Bottke et al. (2002), the authors estimated the true (debiased) distribution of asteroid orbits in the proximity to the Earth, see Figure 1.4. It is evident that the observed population is biased in several ways, for example it is easier to discover an asteroid with eccentricity ≤ 0.4 than with a larger value. The authors scaled the predicted distribution to the observed one by Spacewatch[3] and estimated the total number of 960 ± 120 near-Earth asteroids with $H < 18$ (~ 1 km asteroids) and with Tisserand parameter[4] < 2. In December 2000, over 44%

[3]For more information, visit "http://spacewatch.lpl.arizona.edu".

[4]Tisserand parameter $T = \frac{a_J}{a} + 2\sqrt{(1-e^2)\frac{a}{a_J}}\cos i$, where a_j is the semi-major axis of

of the estimated population was discovered. In January 2020, 1059 of such near-Earth asteroids are known (according to`JPL Small-Body Database`) making it almost a complete population, even when considering the upper estimation limit.

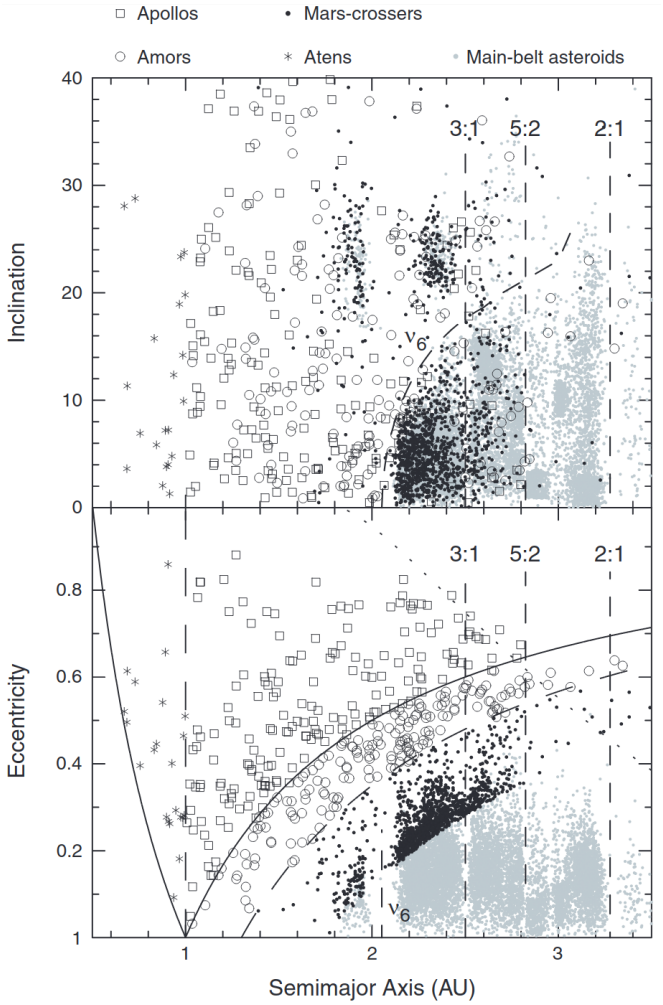

Figure 1.3: The orbital distribution of near-Earth objects, Mars-crossers (black dots) and 10 000 Main Belt asteroids (grey dots). The near-Earth objects are split into three groups based on their semi-major axis a, perihelion q or aphelion Q: Amors with 1.017 AU $< q <$ 1.3 AU (circles), Apollos with $a >$ 1.0 AU and $q <$ 1.017 AU (squares) and Atens with $a <$ 1.0 AU and $Q >$ 0.983 AU (asterisks). The solid curved line represents the Earth-crossing region, the dashed curve delimits the Amor region at $q =$ 1.3 AU, and the dashed vertical line denotes the boundary between the Aten and Apollo populations. Figure taken from Morbidelli et al. (2002).

1.1.2 Physical properties of asteroids

Rotational state of asteroids

It is evident from Figure 1.5 that asteroids with diameter $D >$ 0.15 km only rotate with rotational periods longer than $\sim$ 2 hours. This is closely related

Jupiter and (a, e, i) are standard orbital elements of a given object.

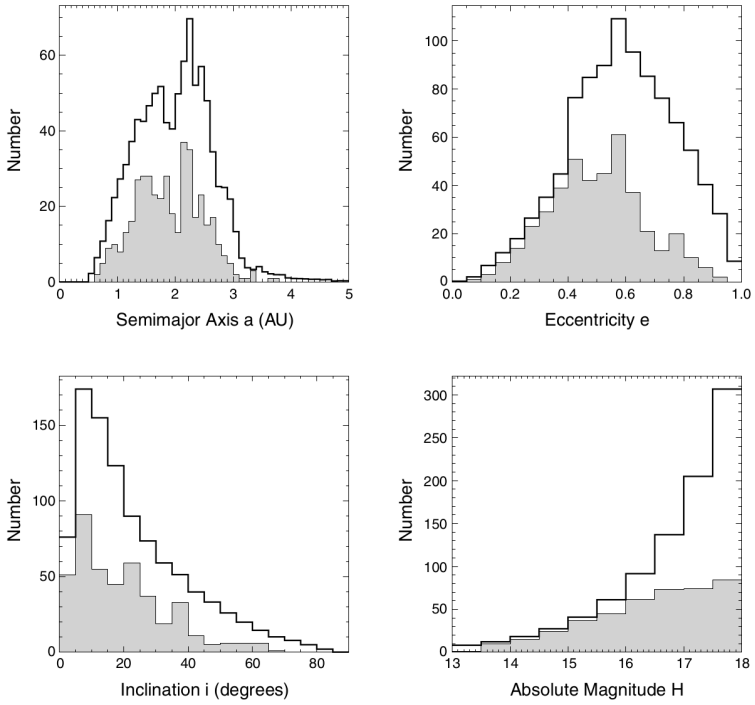

Figure 1.4: The orbital distribution of the observed population of near-Earth objects (black line) and the bias-corrected distribution prediction (shaded histogram) for asteroids with $H < 18$. Figure taken from Bottke et al. (2002).

to the internal structure, which is not monolithic, but the body is shattered or a rubble pile (Richardson et al., 2002). Once an asteroid reaches its critical rotational frequency, its own gravity is not sufficient enough to keep the body (composed of fragments) together. However, for the smallest asteroids, we see rotational periods much shorter than 2 hours (in an order of minutes). These are probably fragments of asteroid collisions.

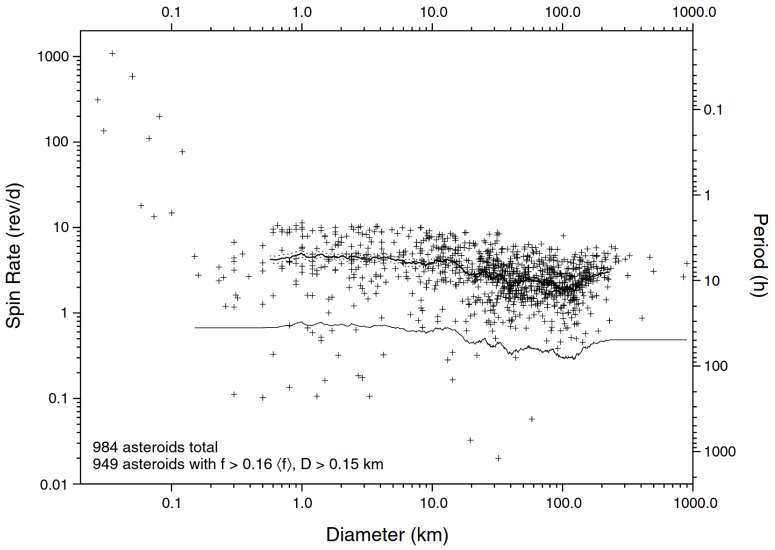

Figure 1.5: Asteroids' spin rate vs. their diameter. Only asteroids with $D < 0.15$ km are observed to rotate with periods shorter than 2 hours. Figure taken from Pravec et al. (2002).

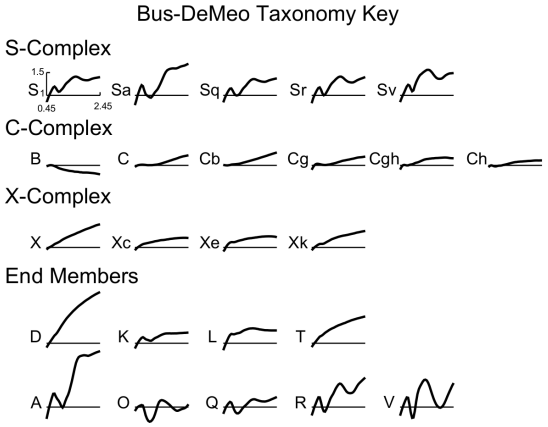

Figure 1.6: The averaged spectra ranging from 0.45 μm to 2.45 μm for the 24 spectral classes of the Bus-DeMeo taxonomy. Image taken from (DeMeo et al., 2015).

Taxonomic classification of asteroids

Based on the reflectance spectra characteristics (measured from 0.45 to 2.45 μm) of 371 asteroids, DeMeo et al. (2009) extended the visible wavelength taxonomy from Bus (1999) into the near-infrared part of the spectrum. They were able to preserve 23 Bus's taxonomy classes, while they eliminated 3 (Ld, Sk, Sl) and created one new class (Sv), see Table 2 in DeMeo et al. (2009). An overview of the averaged spectra for all the 24 DeMeo classes is shown in Figure 1.6. Here, we will mention only the basic taxonomic complexes with estimated mean albedo $\overline{p_V}$ values from Usui et al. (2013) and estimated densities ρ from Carry (2012). The complexes are

- **S-complex** - [S, Sa, Sq, Sr, Sv] classes, moderate slope of spectrum with notable 1μm and typically also 2μm spectral feature caused by olivine and pyroxene minerals, $\overline{p_V} = 0.208 \pm 0.079$ and ρ from 2.72 ± 0.54 to 3.43 ± 0.20 g/cm^3

- **C-complex** - [B, C, Cb, Cg, Cgh, Ch] classes, flat or low sloped spectrum with no or weak features, carbon and phyllosilicates minerals present likely due to aqueous alteration, $\overline{p_V} = 0.071 \pm 0.040$, ρ from 1.25 ± 0.21 to 1.41 ± 0.29 g/cm^3

- **X-complex** - [X, Xc, Xe, Xk] classes, moderate slope of spectrum with no or very weak features, $\overline{p_V} = 0.098 \pm 0.081$, but can vary significantly (p_V to to 0.5), $\rho = 1.85 \pm 0.81$ to 4.86 ± 0.81 g/cm^3, compositionally degenerated surface

- **Other** - [T, D, Q, O, R, V, A, K, L] classes, end members and outliers, for information about specific types, see DeMeo et al. (2009, 2015).

Interestingly, for the S- and the C- complexes, asteroids with more mass tent to have higher density, which is probably caused by a lower macroporosity of more massive asteroids (Carry, 2012).

1.2 Orbital description

The position and trajectory of asteroids in our Solar System are usually described in a heliocentric ecliptic J2000 reference frame by six orbital elements, which are

- a – semi-major axis of an orbital ellipse;
- e – eccentricity of the orbital ellipse, describing its elongation;
- i – inclination of orbit with respect to the ecliptic plane;
- Ω – longitude of the ascending node, measuring the angular distance of the ascending point from the reference frame's vernal point;
- ϖ – longitude of perihelion, sum of Ω and argument of perihelion ω, which measures the angular distance between the ascending node line and the perihelion;
- M – mean anomaly describing angular position of asteroid in a given time if it was at circular orbit with the same orbital period, measured from asteroid's perihelion.

1.2.1 Osculating orbital elements

Since our Solar System does not include only the Sun – greatest source of gravitational interaction – but also planets, which cause gravitational perturbations, the orbital elements of objects in the Solar System are not constant and change over time. Therefore, it is necessary to state for what time, epoch, the orbital elements are stated. A full set of osculating orbital elements consist of six orbital elements, which were calculated as if only the Sun was interacting with the asteroid (all the planets and other mass bodies were ignored) and the corresponding epoch. Thus, if we compare two orbits described by osculating orbital elements, it is necessary for the two epochs to be the same (and also the reference frame, of course). The osculating orbital elements accurately describe asteroid's current orbit and position in space, but are not very representative for the asteroid's orbital history.

1.2.2 Mean orbital elements

As mentioned in the previous section, osculating orbital elements do not represent asteroids orbital history (on the scale of 10^3 years and longer) very well. Therefore, they are not very suitable for finding orbital associations among asteroids and events that happened $10^4 - 10^6$ years ago. Fortunately, most of the asteroids in the Main Belt (where the vast majority of known asteroids is located) are at stable orbits (meaning that they did not experience a close encounter with a massive object that would significantly alter their orbit or are in a strong orbital resonance with a planet). In such case, the perturbations caused by planets are periodical and the short time oscillations can be filtered out while investigating asteroid's orbital history. Mean orbital elements are obtained by removing short periodic perturbations from the osculating orbital elements. For a detailed description of how mean orbital elements are calculated, we refer the reader to

Milani and Knežević (1998). Mean orbital elements are ideal for identifying products (new asteroids) of events that happened in the last few million years, such as collisions or disruptions of asteroids.

1.2.3 Proper orbital elements

Even the mean orbital elements are influenced by perturbations causing their variation over a long time. The removal of perturbations with long periods leads to proper orbital elements. Proper elements are constant for at least $10^6 - 10^7$ years depending on the orbit's proximity to orbital resonances. Proper elements are suitable to identify asteroid families that were formed $10^7 - 10^9$ years ago (see e.g., Spoto et al., 2015), which are notable in Figure 1.2. For more information, we refer the reader to Knežević et al. (2002); Knežević (2017).

1.3 Yarkovsky and YORP effects

Asteroid orbits are strongly influenced by the gravity of massive objects, such as the Sun, planets, dwarf planets and even large asteroids (during a close encounters). However, there are also non-gravitational effects that can play a role in asteroids orbital evolution as well as in their rotational state. In the following two chapters, we will briefly describe the two most significant effects (at least for the study of asteroid pairs and clusters). A great summarising article regarding the Yarkovsky and the YORP effect was published recently in `Asteroids IV` (Vokrouhlický et al., 2015) and many information in the two following chapters were drawn from it.

1.3.1 Yarkovsky effect

The Yarkovsky effect is a thermal effect caused by the Sun's radiation. The part of an asteroid (or any object) that is exposed to the sunlight heats up and the surface temperature is slightly higher then the temperature at the dark (unilluminated) side. Since every object with a non-zero temperature emits a thermal radiation, the illuminated asteroid emits radiation from its whole surface. But since the temperature is not the same across the whole surface and since photon's momentum depends on their wavelength, a small thrust caused by the emitted different-momentum thermal photons appears. The Yarkovsky effect requires that a thermal gradient appears on the surface, thus for a very small body or body with near infinite heat conductivity the Yarkovsky effect would not appear. It has been shown that the absorbed and directly reflected sunlight does not produce a long-term dynamical effects (Vokrouhlický et al., 2000; Žižka and Vokrouhlický, 2011), therefore, a non-zero thermal inertia is required for the Yarkovsky effect to appear.

Fortunately, the shape of an object is not essential for the Yarkovsky effect and even a spherical model is a good approximation. The most notable change of asteroid's orbit under the influence of Yarkovsky effect is in the semi-major axis (a). A simple analytical model assumes a circular orbit around the Sun, a fixed orientation of the rotational axis in the inertial space and a linearization of the surface boundary condition. The averaged change in a after one complete orbit is

composed of two contributions (e.g., Rubincam, 1995, 1998; Farinella et al., 1998; Vokrouhlicky, 1998; Vokrouhlický, 1999), the diurnal effect

$$\left(\frac{da}{dt}\right)_{\text{diunar}} = -\frac{8}{9}\frac{\alpha\Phi}{n}W\left(R_\omega, \Theta_\omega\right)\cos\gamma \tag{1.1}$$

and the seasonal effect

$$\left(\frac{da}{dt}\right)_{\text{seasonal}} = \frac{4}{9}\frac{\alpha\Phi}{n}W\left(R_n, \Theta_n\right)\sin^2\gamma\,, \tag{1.2}$$

where $\alpha = 1 - A$, A being the Bond albedo, γ is the spin axis obliquity, n is the orbital mean motion, $\Phi = \pi R^2 F/\left(mc\right)$, where R is the radius of the body, F is the solar radiation flux at the orbital distance from the Sun, m is the mass of the body, c is the speed of light and $W\left(R_\nu, \Theta_\nu\right)$ is a function determined by the thermal parameters (e.g., thermal conductivity, surface density, surface heat capacity, thermal emissivity) of the body and frequency ν, where $\nu = \omega$ for the diurnal component and $\nu = n$ for the seasonal component of the Yarkovsky effect.

We point out the different dependency of the diurnal and seasonal effect on γ. The diurnal effect $\propto \cos\gamma$, which means that it can cause positive or negative change in a. It reaches its maximal strength when the body's rotational axis is perpendicular to its orbital plane ($\gamma = 0°$ or $180°$) and disappears when the rotational axis lies in the orbital plane ($\gamma = 90°$). On the other hand, the seasonal effect $\propto \sin^2\gamma$, which results only in spiraling towards the Sun, with exception when the rotational axis is perpendicular to the orbital plane ($\gamma = 0°$ or $180°$), then it is zero. This means that the seasonal effect reaches maximum, when the diurnal effect is zero ($\gamma = 90°$). For a more complete explanation and derivation see e.g., Vokrouhlický (1999); Vokrouhlický and Bottke (2001); Bottke et al. (2006); Vokrouhlický et al. (2015) and for detection of Yakrovksy effect on several asteroids, see e.g., Chesley et al. (2003, 2016); Vokrouhlický et al. (2008a).

1.3.2 Yarkovsky–O'Keefe–Radzievskii–Paddack effect

The Yarkovsky–O'Keefe–Radzievskii–Paddack (YORP) effect is also, similarly as the Yarkovsky effect, a non-gravitational effect caused by the Sun's radiation. In this case, both the directly scattered visible light and the thermally emitted radiation cause dynamical changes over a long time. In principle, these two components of the YORP effect should be treated separately, since they can each produce a different torque acting on the body. The YORP effect can both, increase or decrease the rotational rate of an object, but it tends to change the obliquity towards $0°, 90°$ or $180°$. Unlike the Yarkovsky effect, the YORP effect depends heavily on the object's shape and even the middle- to small- sized irregular surface features can play a significant role (even dominat role) in the total strength of the YORP effect. This strong dependency on shape and irregularities makes the modelling quite difficult, since the YORP effect does not act on bodies with simple, symmetrical shape.

Two semi-analytical approaches were taken in years 2007 and 2008[5] and after averaging over a complete rotation and revolution cycle, both models predicted

[5]Scheeres (2007); Scheeres and Mirrahimi (2008) started the description of YORP with polyhedral shaped object, whereas Nesvorný and Vokrouhlický (2007, 2008); Breiter and Michalska (2008) described the shape as as series expansion in spherical harmonics.

a change of objects rotational rate ω as

$$\frac{d\omega}{dt} = \frac{\Lambda}{C} \sum_{n \geq 1} A_n P_{2n}(\cos\gamma) \tag{1.3}$$

and its obliquity γ as

$$\frac{d\gamma}{dt} = \frac{\Lambda}{C\omega} \sum_{n \geq 1} B_n P^1_{2n}(\cos\gamma), \tag{1.4}$$

where $\Lambda = 2FR^3/(3c)$ (for reminder, R is the radius of the body, F is the solar radiation flux at the orbital distance from the Sun), C is the moment of inertia corresponding to the rotational axis, A_n and B_n are non-dimensional coefficients determined by the shape of the body, $P^1_{2n}(\cos\gamma)$ are the Legendre polynomials of even degrees and $P^1_{2n}(\cos\gamma)$ are the corresponding associated functions. Since $C \propto R^5$, the strength of the YORP effect $\propto 1/R^2$ and therefore the rotational state of smaller objects can be much more influenced (on shorter timescales) by the YORP effect than the rotational state of large objects. Since the publication of these models, a big progress was made and we refer interested readers to e.g., Breiter and Vokrouhlický (2011); Vokrouhlický et al. (2015); Bottke et al. (2015). The YORP effect has been already detected for several asteroids, see e.g. Lowry et al. (2007); Kaasalainen et al. (2007); Ďurech et al. (2008).

1.4 Formation of asteroid pairs and clusters

Asteroid pairs are two asteroids orbiting around the Sun on very similar heliocentric orbits. With the growing number of the asteroid pairs with very similar orbits (currently on an order of hundreds), it is extremely unlikely that they occurred only by chance. It is believed that the two components of an asteroid pair come from the same parent asteroid, which was disrupted (probably via a rotational fission) and the fragments got out of the respective gravitational reach at very low relative velocities (e.g., Scheeres, 2007). If we find more then two asteroids with very similar heliocentric orbits, also suspecting disruption by rotational fission, we used the term asteroid cluster.

Even though the strength of the YORP effect is very small over a short period of time, at larger timescales (millions of years or even shorter) it can cause a significant change to the rotational state of an asteroid. If the YORP effect keeps increasing asteroid's rotational frequency, it will eventually reach a critical spin rate[6] and it will undergo a disruption. That is the reason, why there are no fast rotators among asteroids with $D >\sim 0.15$km, see Figure 1.5. For simplicity, we will further assume a case in which an asteroid is split-up into two pieces. There are many evolution paths (depending mainly on the mass ratio of new fragments) with different final states of this newly formed system see Figure 1.7. If the free energy E_{free} of the system is positive, then it is possible for the smaller fragment (secondary) to escape from the gravitational reach of the large fragment (primary)

[6]Critical spin rate depends on objects shape, total mass and its distribution, friction coefficients and its angle etc. For a homogeneous sphere with density ρ and the angle of friction of 90° the critical spin rate is $\omega_{\text{crit}} = \sqrt{4/(3\pi G\rho)}$ (Pravec et al., 2010, *Supplementary Information*).

- the system becomes unbound. The free energy of a system of two bodies can be expressed as

$$E_{\text{free}} = \underbrace{\frac{1}{2}\omega_{\mathbf{1}} \cdot \mathbf{I_1} \cdot \omega_{\mathbf{1}}}_{E_{\text{rot}} \text{ of ast. 1}} + \underbrace{\frac{1}{2}\omega_{\mathbf{2}} \cdot \mathbf{I_2} \cdot \omega_{\mathbf{2}}}_{E_{\text{rot}} \text{ of ast. 2}} + \underbrace{\frac{1}{2}\frac{m_1 m_2}{m_1 + m_2}\mathbf{v} \cdot \mathbf{v}}_{\text{Translat. kinetic energy}} + \mathcal{U}_{12}, \tag{1.5}$$

where $\omega_{\mathbf{1}}, \omega_{\mathbf{2}}$ are angular velocities of the two bodies, $\mathbf{I_1}, \mathbf{I_1}$ are rotational inertia of the two bodies, m_1, m_2 are their corresponding masses, $\mathbf{v}$ is the relative velocity vector between these two components and $\mathcal{U}_{12}$ is the mutual potential[7] between the two bodies. If the system becomes unbound (positive E_{free} does not mean that the system must become unbound), then $\mathcal{U}_{12}$ reaches zero and $\mathbf{v}$ will approach velocity of a hyperbolic escape, therefore, $\mathbf{v} \cdot \mathbf{v}$ becomes v_∞^2 (drawn from Pravec et al., 2010). Additionally, the increase of the negative $\mathcal{U}_{12}$ to zero needs to be compensated by energy decrease of the other component. Due to the v_∞ being small, the whole term corresponding to the translation kinetic energy in Equation 1.5 becomes very small. And because the secondary is typically much smaller than the primary, it holds much less rotational energy (E_{rot}) than the primary. Therefore, in order for the secondary to be able to escape, the primary's rotational energy needs to be decreased, resulting in its slowed down rotation.

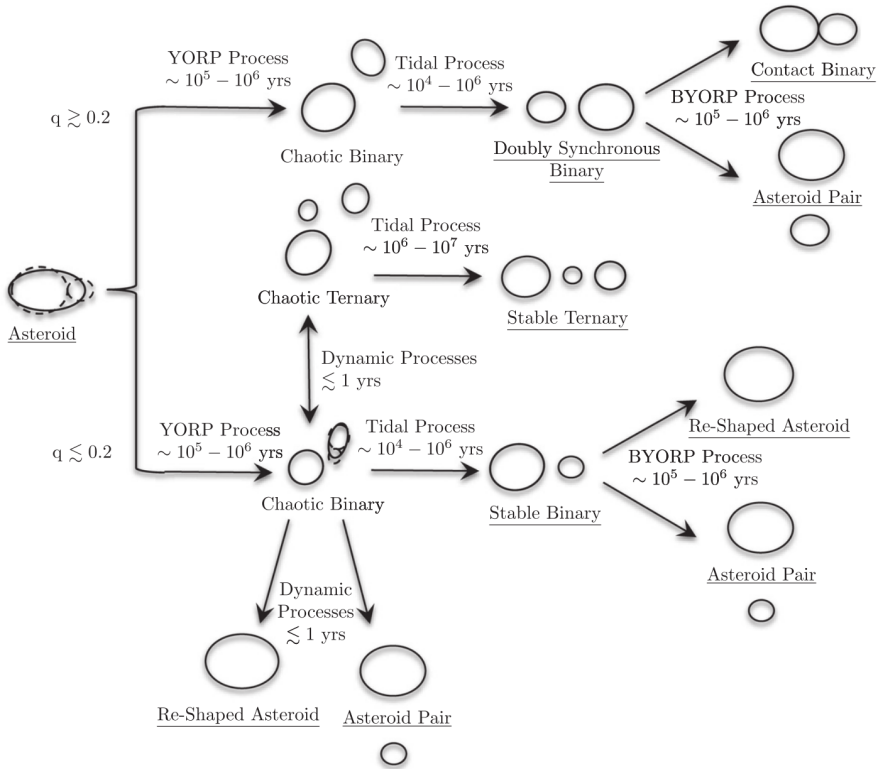

Figure 1.7: Illustration of several evolutionary paths of a disrupted asteroid resulting in different final configurations. Arrows indicate the direction of evolution along with the process propelling the evolution and a typical timescale. Figure taken from Jacobson and Scheeres (2011).

[7] $\mathcal{U}_{12} = -G \int_{\beta_1} \int_{\beta_2} \frac{dm_1 dm_2}{|\boldsymbol{\rho_1}\boldsymbol{\rho_2}|}$, where β_1, β_2 represents the mass distribution of the two objects, $\boldsymbol{\rho_1}, \boldsymbol{\rho_2}$ are the locations in the bodies of a mass elements dm_1 and dm_2, respectively.

To estimate the angular velocity of a primary after an escape of a secondary created by a rotational fission, Pravec et al. (2010) created a model of a proto-binary separation. Their model started with a close binary asteroids (already after fission) and the final evolution state was a barely escaping secondary. The model assumes a conservation of the free energy as well as the total angular momentum close to the critical value (normalized total angular momentum[8] $\alpha_L \sim 1$), that the spin vectors of components are coplanar with their mutual orbit and that the secondary rotates with a constant period. Then the free energy is

$$E_{\text{free}} = \frac{1}{2} I_1 \omega_1^2 + \frac{1}{2} I_2 \omega_2^2 - G \frac{m_1 m_2}{2A}, \tag{1.6}$$

where index "1" denotes a physical quantity related to the primary and index "2" to the secondary and A is the orbital semi-major axis of the system. Because E_{free} remains constant in this model, for the initial (subscript "ini") and the final (subscript "fin") state (with $A_{\text{fin}} \to$ infinity), we can write

$$\underbrace{\frac{1}{2} I_1 \omega_{1\ \text{ini}}^2 + \frac{1}{2} I_1 \omega_{2\ \text{ini}}^2 - G \frac{m_1 m_2}{2A_{\text{ini}}}}_{\text{initial state}} = \underbrace{\frac{1}{2} I_1 \omega_{1\ \text{fin}}^2 + \frac{1}{2} I_1 \omega_{2\ \text{fin}}^2}_{\text{final state}}. \tag{1.7}$$

And since we assumed that $\omega_{2\ \text{ini}} = \omega_{2\ \text{fin}}$, it is easy to obtain a relation for $\omega_{1\ \text{fin}}$. By substituting $I_1 = m_1(a_1^2 + b_1^2)/5$ for a rotating ellipsoid with axes a_1, b_1, c_1 with the c_1 axis being identical with the rotational axis, we get

$$\omega_{1\ \text{fin}}^2 = \omega_{1\ \text{ini}}^2 - 5G \frac{m_2}{(a_1^2 + b_1^2)\, A_{\text{ini}}}. \tag{1.8}$$

As we expected, larger mass of escaping secondary translates to more pronounced slow down of the primary's rotation (assuming fixed a_1 and b_1). We usually do not know M_2, but we can estimate the mass ratio between the primary and the secondary $q = M_2/M_1 = 10^{-0.6(H_2 - H_1)}$ and to get fewer variables in our equations, we substitute $M_1 = \rho \frac{4}{3} \pi a_1 b_1 c_1$ and after some rearrangement, we get

$$\omega_{1\ \text{fin}}^2 = \omega_{1\ \text{ini}}^2 - \frac{20\pi}{3} \frac{G q \rho a_1 b_1 c_1}{(a_1^2 + b_1^2)\, A_{\text{ini}}}. \tag{1.9}$$

Finally, ω_{ini} can be calculated using the assumption of total angular momentum of the system conservation (see Pravec et al., 2010, *Supplementary Information* for full derivation).

Model described above assumes only two components of the system, but it can be generalized for N bodies (such as asteroid clusters) with the assumption that the total mass of all secondaries (with indexes starting from "2" up to "N") is much smaller then the the mass of the primary (with index "1"). Following Pravec et al. (2018), this assumption is mathematically expressed as

$$q \equiv \sum_{j=2}^{N} \frac{M_j}{M_1} \ll 1. \tag{1.10}$$

[8] $\alpha_L = \frac{L_1 + L_2 + L_{\text{orb}}}{L_{\text{eqsph}}}$, where L_1 and L_2 are rotational angular momentum of the primary and the secondary, respectively, L_{orb} is the orbital angular momentum, and L_{eqsph} is the angular momentum of the equivalent sphere spinning at the critical spin rate.

The free energy can be then calculated as

$$E_{\text{free}} \doteq \frac{1}{2} I_1 \omega_1^2 + \sum_{j=2}^{N} \left(\frac{1}{2} I_j \omega_j^2 - G \frac{m_1 m_j}{2A_j} \right). \tag{1.11}$$

The equation for computing $\omega_{1\ \text{fin}}$ remains unchanged from the equation 1.9. This models give us a prediction for the primaries' rotational periods. Pravec et al. (2010) verified this prediction for a few dozens of asteroid pairs, see Figure 1.8. In Pravec et al. (2019), we supported the validity of this prediction by increasing the number of tested pairs to 93, see Section 3.2 and in Pravec et al. (2018), we performed the same comparison to a set of 13 asteroid cluster, see Section 3.1.

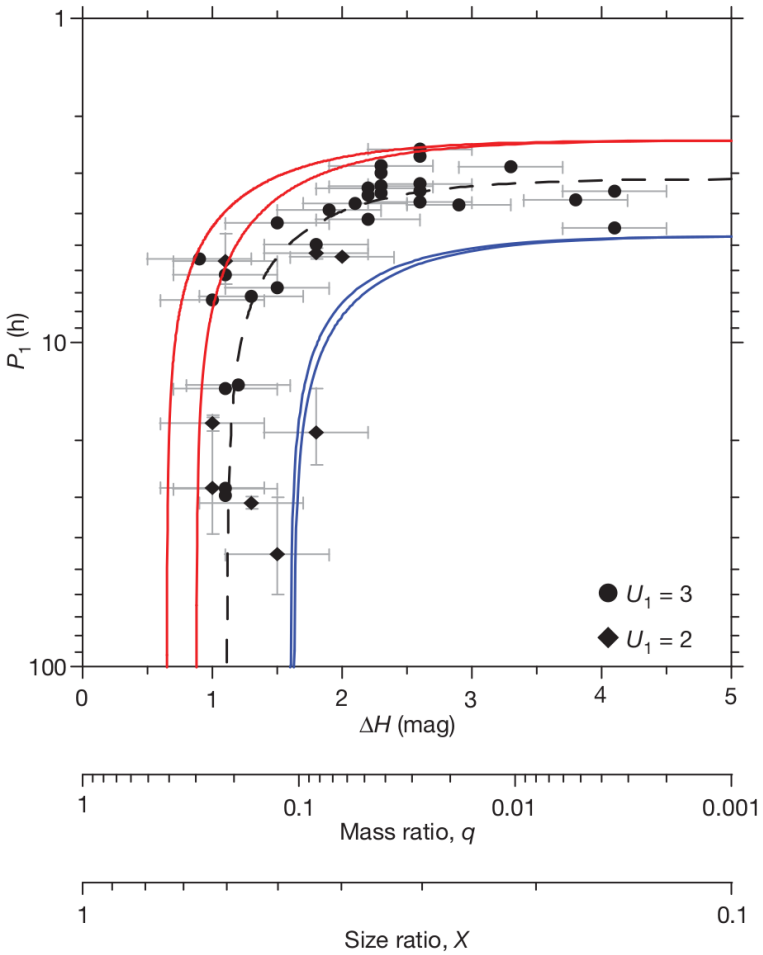

Figure 1.8: Rotation periods of primaries vs. the mass ratios q of the secondary and the primary for asteroid pairs. Blue and red lines indicates the limits for values still allowed by the model described in 1.4 and the black dashed line represents the predicted dependency for a set of parameters best representing the properties of the pair ($\alpha_L = 1.0$, a primary axial ratio $a_1/b_1 = 1.4$ and an initial orbit's normalized semi-major axis $A_{\text{ini}}/b_1 = 3$). For more information see Pravec et al. (2010) from where was this figure taken.

2. Identification methods of asteroid pairs and clusters

According to `JPL Small-body Database Search Engine`, there are currently (as of January 2020) ∼541 000 numbered and nearly 390 000 unnumbered asteroids in our Solar System. To find groups consisting of two or a few asteroids that used to be part of a single body (asteroid pairs and clusters) and broke-up in the recent history (typically less than a few million years), sophisticated methods needed to be employed to search through the whole database of over 930 000 known asteroid orbits. For the vast majority of the known asteroids, we have only information about their orbits and typically a rough estimation of their absolute magnitudes (Pravec et al., 2012, showed that there are systematic offsets among asteroid orbit catalogs, especially for asteroids with $H > 12$). Therefore, a search for genetically related asteroids should be primarily based on orbit comparison. This makes also sense if we consider that at the time of separation, asteroid pair/cluster members shared the same location and their relative velocities were very low compared to the orbital velocity. To quantify the similarity of two orbits, we used an extended[1] five-dimensional version (e.g., Nesvorný and Vokrouhlický, 2006; Pravec and Vokrouhlický, 2009) of a three-dimensional metric introduced by Zappala et al. (1990). This enables us to compute the distance d [m/s] of any two orbits (assuming ellipsoidal orbits with the same focus) in the five-dimensional space of osculating or mean orbital elements (a, e, i, Ω, ϖ) defined as a positive-definite quadratic form

$$\left(\frac{d}{na}\right)^2 = k_a \left(\frac{\delta a}{a}\right)^2 + k_e \left(\delta e\right)^2 + k_i \left(\delta \sin i\right)^2 + k_\Omega \left(\delta\Omega\right)^2 + k_\varpi \left(\delta\varpi\right)^2 , \qquad (2.1)$$

where n is the mean motion, a is the arithmetic average of semi-major axes of the two orbits, $(\delta a, \delta e, \delta \sin i, \delta\Omega, \delta\varpi)$ is the separation vector of the orbits and the coefficients are $k_a = 5/4, k_e = k_i = 2, k_\Omega = k_\varpi = 10^{-4}$.

2.1 Statistical significance method

Pravec and Vokrouhlický (2009) developed a method for identifying asteroid pairs based on their statistical significance with respect to their mutual distance $d_{\rm pair}$ and the orbital background density in their vicinity. Here we adopt similar notation as the authors. To estimate the statistical significance of a given pair (with $d_{\rm pair}$), it is necessary to estimate the expected number of pairs $P_2\left(d_{\rm pair}\right)$ with $d \leq d_{\rm pair}$ in a given volume V of the population around given pair and the total number of pairs with $d \leq d_{\rm pair}$ (N_p). The probability is then simply P_2/N_p. The equation for computing $P_2\left(d\right)$ can be derived from the formula of Poisson distribution. The probability of finding two orbits from a population with the

[1] Extended by terms involving orbital elements Ω and ϖ, where the coefficients k_Ω and k_ϖ were chosen empirically.

number density η within a volume V is then

$$p_2(V) = \frac{\nu^2}{2!} e^{-\nu}, \tag{2.2}$$

where $\nu = \eta V$. We obtain the expected number of pairs in M cells of volume V as

$$P_2(V) = M p_2(V) = M \frac{\nu^2}{2} e^{-\nu}. \tag{2.3}$$

The total number of pairs in M cells is simply $N = \eta V M = \nu M$ and substituting M in equation (2.3) with $M = N/\nu$, we get

$$P_2(V) = \frac{N\nu}{2} e^{-\nu}. \tag{2.4}$$

It is more convenient to have P_2 dependant explicitly on d rather then on V. To achieve this, we use a relation between a radius d and a volume V of a five-dimensional hypersphere, which is

$$d = \left(\frac{8\pi^2}{15} \frac{1}{V} \right)^{-1/5}. \tag{2.5}$$

Replacing the $1/V$ in equation (2.5) with η, we obtain a characteristic distance of objects for the observed density η in specific volume, therefore

$$R_0 = \left(\frac{8\pi^2}{15} \eta \right)^{-1/5}. \tag{2.6}$$

And since $\nu = \eta V = (d/R_0)^5$, we can rewrite equation (2.4) as

$$P_2(V) = P_2(d) = \frac{N}{2} \left(\frac{d}{R_0} \right)^5 e^{-\left(\frac{d}{R_0}\right)^5}. \tag{2.7}$$

In Fatka et al. (2020), where we studied four asteroid clusters, we estimated the probability (p_1) that the most distant cluster member from the primary was falsely identified as a cluster member and is actually only a background asteroid (an interloper). Any closer cluster members always have lower probability of being an interloper, therefore, we limited our estimation only to the farthest member of each cluster (with distance from the primary d). The probability of an interloper being within the volume $V(d)$ around the primary is then

$$p_1(V) = \frac{\nu}{1!} e^{-\nu}. \tag{2.8}$$

Using the relation $\nu = (d/R_0)^5$ we obtain

$$p_1(d) = \left(\frac{d}{R_0} \right)^5 e^{-\left(\frac{d}{R_0}\right)^5}. \tag{2.9}$$

In many cases, the ratio $(d/R_0)^5 \ll 1$, thus the probability estimation simplifies to

$$p_1(d) = \left(\frac{d}{R_0} \right)^5. \tag{2.10}$$

Both of the two above probability estimations assume that the distribution of the background orbits is uniform. This assumption is not met when, for example, a studied pair/cluster is located near a mean motion resonance or in the proximity of a large asteroid family.

2.2 Backward orbital integration method

To confirm a common origin of asteroid pair or cluster members indicated by the asteroids mutual distance in the space of orbital elements, we performed a backward orbital integration of candidate members. Each of the candidates was represented by a few hundreds or a few thousands[2] of geometric clones with Yarkovsky effect acting on each clone differently. This test provides an age estimation of a given pair or cluster and in the case of close and slow encounters (see section 2.2.3) it can even identify potential interlopers. However, the extent of this method's usability is limited by the long-term orbital stability of given asteroids. A close encounter with a major planet or a massive asteroid significantly increases the unpredictability of orbits' evolution similarly as resonances caused by major planets. This method is typically suitable for integration up to a few million years in the Main Belt of asteroids, but for near-Earth objects, the orbital predictability is shorten significantly, typically below 100 kyr.

Since every orbit is known with only a finite accuracy and an orbital propagation of objects in our Solar System through time depends heavily on initial conditions, we create geometric clones of given asteroids to cover as many different orbital realizations as possible. These clones have initially very similar orbital elements, but diverge over time. The initial orbital elements $\mathbf{E}$ of these geometric clones are created with the use of the best-fit orbit solution $\mathbf{E}^*$ and its covariance matrix Γ in the six-dimensional space of non-singular equinoctial orbital elements (a, k, h, q, p, λ) provided by `AstDyS-2` website[3]. Following Milani and Gronchi (2010), the probability density function $p(\mathbf{E})$ in six dimensions is

$$p(\mathbf{E}) = \frac{\sqrt{\det \mathrm{C}}}{(2\pi)^3} \exp\left(-\frac{1}{2}\Delta\mathbf{E}^T \cdot C \cdot \Delta\mathbf{E}\right), \tag{2.11}$$

where $\Delta\mathbf{E} = \mathbf{E} - \mathbf{E}^*$ and C is the normal matrix satisfying $C = \Gamma^{-1}$. Orbital elements $\mathbf{E}$ of each clone were generated as

$$\mathbf{E} = T^T\mathbf{z} + \mathbf{E}^*, \tag{2.12}$$

where $\mathbf{z}$ is a six-dimensional vector with randomly chosen values following the normal distribution and T is a decomposed matrix, which satisfies $T^T T = \Gamma$.

A typical size of known pair and cluster members ranges from a few kilometers to only a several hundreds of meters and therefore, Yarkovsky effect can play a significant role in asteroid propagation in time. Currently, the rotational state (rotational period and orientation of principal axis in space) of the vast majority of known asteroid is unknown. Therefore, in most cases, we have to take into account both the possibilities that an asteroid is "pushed" closer to the Sun or away from it by the Yarkovsky effect. Following Farnocchia et al. (2013), the Yarkovsky effect was represented using a fake transverse acceleration providing secular change in semi-major axis. We estimated the maximum possible semi-major axis drift $\dot{a}_{\max}$ for given asteroids size[4] and its distance from the Sun. Each

[2] In Pravec et al. (2018) we used 500 orbital clones per asteroid, but in following works (after switching to `REBOUND` package) we used at least 1000 clones per asteroid.

[3] Accessible at "https://newton.spacedys.com/astdys/".

[4] The diameter D of an asteroid was estimated based on its geometric albedo p_v and its absolute magnitude H as $D = \frac{1329}{p_v} 10^{-H/5}$ (Harris and Harris, 1997).

of the generated geometrical clones was assigned a random value of a semi-major drift in range $\langle -\dot{a}_{\max}, \dot{a}_{\max} \rangle$.

2.2.1 Test of nominal orbits with Yarkovsky clones

To have a chance of finding slow encounters of two given asteroids during their backward orbital integration (more in section 2.2.3), their orbits need to be coplanar - differences in secular angles Ω and ϖ must be close to zero at the same time. As a quick test of whether two asteroid orbits could be coplanar in the past (asteroids could be related), we performed a backward integration of their nominal orbits (best-fit solutions). We check the time evolution of secular angle differences $\delta\Omega$ and $\delta\varpi$ ($\delta\Omega = \Omega_{\text{ast1}} - \Omega_{\text{ast2}}$ and $\delta\varpi$ analogically) and evaluate whether the secular angles converged in the past around the same time. All cluster members, especially secondaries due to their smaller sizes, are influenced by the Yarkovsky effect, which could play a significant role in the orbit evolution in time. To take the Yarkovsky effect into account in this test (at least partially), we created three Yarkovsky clones[5] for each asteroid and assigned them with zero, the maximum negative and the maximum positive Yarkovsky acceleration possible for given asteroid. Then we checked all nine clone combinations for convergences of $\delta\Omega$ and $\delta\varpi$. The idea behind this method is very similar to the one used by Novaković et al. (2012) named *Selective Backward Integration Method*, which helps to distinguish between real cluster members and background asteroids.

Apart from the indication whether two asteroids could be genetically related or not, the test also provides a constraint for their possible age. With the inclusion of the three Yarkovsky clones per each asteroid, in one of the nine clone combinations, we simulate the fastest possible convergence rate of Ω and ϖ. And since coplanarity is a necessity (in the theory of rubble-pile asteroid break-up induced via rotational fission), we can set a lower limit on the time of separation of these two components. This test works well for asteroid pairs and clusters, whose orbits had enough time to diverge. For very young pairs the secular angles are still very similar and due to the perturbations from major planets (with amplitudes in Ω and ϖ up to 1°), we are typically unable to put any constraint regarding their age.

2.2.2 Secular angles convergence

In backward orbital integrations with many probable asteroid members (leading to the use of smaller number of orbital clones) or in cases with higher orbital chaoticity, we can limit our examination to the convergences of secular angles (Ω, ϖ). This method searches for moments, when the angles Ω and ϖ are similar among all the cluster members. In Pravec et al. (2018), we employed a function $\Delta V\,(t)$ introduced by Nesvorný and Vokrouhlický (2006) and we searched for its minimum (for time t when its value was below a set threshold). The function reads

$$\Delta V\,(t) = na\sqrt{k_1\left(\sin i \Delta\Omega\right)^2 + k_2\left(e\Delta\varpi\right)^2}, \tag{2.13}$$

[5] Yarkovsky clones share the same initial orbital elements, but have different Yarkovsky effect strength acting on them.

where $k_1 = 1$, $k_2 = 1/2$ and the dispersion of secular angles $(\Delta\Omega, \Delta\varpi)$ at time t is defined as

$$(\Delta\Omega)^2 = \frac{\Sigma_{ij} \left(\Delta\Omega_{ij}\right)^2}{N\left(N-1\right)/2} \quad ; \quad (\Delta\varpi)^2 = \frac{\Sigma_{ij} \left(\Delta\varpi_{ij}\right)^2}{N\left(N-1\right)/2} \tag{2.14}$$

where $\Delta\Omega_{ij}$ and $\Delta\varpi_{ij}$ are the differences between Ω and ϖ, respectively, for the i-th and j-th orbit and N is the number of members in the cluster. The disadvantage of this method is that it is unable to discover interlopers, especially among many real cluster members.

2.2.3 Close and slow encounters

The method searching for close and slow encounters between the orbital clones of asteroid pair or cluster members is more challenging than the method described in previous section. It requires the clones to be close to each other (within the set limit $r_{\max}$) while their relative velocity needs to be low (within the set limit $v_{\max}$) as well. The motivation for these two requirement is following – a parent asteroid was split into two or more asteroids so they were physically close to each other at that time. And since the secondary cannot temporarily orbit around the primary at distances greater than the radius of the Hill sphere[6] $R_{\rm Hill}$ of the primary, the secondary must escape at distance comparable to $R_{\rm Hill}$, which is typically a few hundred kilometers for the primaries of studied asteroid pairs and clusters. Since the theory of a rotational fission of a rubble pile asteroid (Scheeres, 2007; Pravec et al., 2010) predicts a gentle escape of a secondary at relative velocities $v_{\rm rel}$ comparable with the escape velocity[7] $v_{\rm esc}$ from the primary's surface, we require $v_{\rm rel}$ of the two clones during an encounter to be similarly low.

In practice, we relax the limits $r_{\max}$ and $v_{\max}$ and set them to higher values that what our hypothesis of formation mechanism suggests. This is justified by several facts, some of them are: (*i*) We do not know the real initial orbits of given asteroids, therefore, we create a set of orbital clones. But, these clones do not follow the exactly same trajectory as the real asteroid followed and their encounter distance and velocity might be "a bit off". (*ii*) The accuracy of asteroid's physical parameters is limited. The uncertainty in H estimations propagates into the $R_{\rm Hill}$ and $v_{\rm esc}$ calculations. And since a rotational period and a lightcurve amplitude are typically unknown, the real uncertainty of H estimation can by much higher than the formal ones. (*iii*) Yarkovsky effect is unknown in most cases, which means that even asteroids with identical initial orbits would follow different trajectories under the influence of different strength the Yarkovsky effect. (*iv*) Precision of N-body integrators is finite. For backward integrations up to 1.5 Myr, we typically use limits $v_{\max} = 2\ v_{\rm esc}$ and $r_{\max} = 5\ R_{\rm Hill}$ and for longer integration, we increase the limits to $v_{\max} = 4\ v_{\rm esc}$ and $r_{\max} = 10\ R_{\rm Hill}$. These are not strict values and can be adjusted for given situation, i.e., lowered for very young pairs to obtain

[6]The radius of the Hill sphere can be calculated as $R_{\rm Hill} \sim a D_1 \frac{1}{2} \left(\frac{4\pi}{9}\frac{G\rho_1}{\mu}\right)^{1/3}$, where a is the heliocentric semi-major axis, D_1 is the estimated diameter of the primary body, G is the gravitational constant, ρ_1 is the primary's bulk density and μ is the gravitational parameter of the Sun. Taken from Pravec et al. (2010) *Supplementary Information* and typo-corrected.

[7]The escape velocity can be calculated as $v_{\rm esc} \sim D_1 \frac{1}{2} \left(\frac{8\pi}{3} G\rho_1\right)^{1/2}$. Taken from Pravec et al. (2010) *Supplementary Information* and typo-corrected.

only the closest and slowest encounters or increased to account for large initial uncertainties of given asteroids.

In Moskovitz et al. (2019), we performed backward orbital integrations for two near-Earth asteroid pair candidates. But due to the initially large orbital uncertainty (both candidate pairs consisted of at least one single-opposition asteroids), we searched for the minimum orbit intersection distance (MOID) instead of the close clone encounters and we calculated the relative velocity at a given MOID configuration. This approach is a relax version of the one described above, because it does not require two clones to by physically close to each other, only their orbits need to get close at any point (there is no dependency on the mean anomaly).

2.3 Age estimation

The results obtained from integrations described in sections 2.2.2 and 2.2.3 can be anywhere between zero and a several million encounters or convergences and it is not clear how to derive an age from these results. Since the time distribution of recorded encounters/convergences is non-Gaussian, often strongly asymmetric and may have complicated shapes with multiple completely separated maxima (distribution peaks), we apply several values and combinations for $v_{\max}$ and $r_{\max}$ limits and we choose the most optimal ones. The choice of $v_{\max}$ and $r_{\max}$ limits is done in a way that we get the closest and slowest encounters possible while still having a representative number of encounters. Typically for young asteroid pairs and clusters we find much more encounters than for the older once and therefore, we can "push" the limits $v_{\max}$ and $r_{\max}$ to smaller values (e.g., $v_{\max} = v_{\mathrm{esc}}$ and $r_{\max} = 3\ R_{\mathrm{Hill}}$), which helps us to take into account only the values closest to the predicted values by the rotational fission theory. For integration with encounters appearing at times larger than 1–2 Myr, we are typically forced to relax the limits to values up to $v_{\max} = 4\ v_{\mathrm{esc}}$ and $r_{\max} = 15\ R_{\mathrm{Hill}}$ to obtain at least several hundred encounters.

Once we have chosen the most suitable limits for a given case, we use the 50th percentile (median) as an age estimation and for estimating uncertainties, we used the 5th and 95th percentile as a lower and upper estimation, respectively.

3. Published papers

In this section, we discuss accepted papers (in impact journals), in which I contributed. In three papers I am listed as the second author and in one of them as a first author. Highlights of these four publications are presented in a chronological order and are accompanied by additional discussion or information. Original papers can be found in Attachments.

3.1 Asteroid clusters similar to asteroid pairs

In this work, we performed an analysis of 13 asteroid clusters. Ten of these clusters were already known and three clusters were new, discovered as a by-product of our search for new asteroid pairs. The newly discovered clusters were cluster of (11842) Kap'bos with 3 members (formerly identified as a pair), (22280) Mandragora with 19 members and (66583) Nicandra with 5 members. All of the three new clusters were originally found in the space of mean orbital elements as a tight pair using a method described in Section 2.1, while the other cluster members were discovered during the search of the surrounding area with distances d_{mean} up to 100 m/s.

Backward orbital integrations

To further evaluate whether the studied clusters were real or not, especially in cases with only a few members, we performed a backward orbital integration and we searched for secular angles convergence of all the members (see Section 2.2.2). We performed this test to eight clusters for which is was not done (or published) before. We considered the previous results for the remaining five clusters sufficient and not needing repeating. For the numerical integration in this work, we used the `Regularized Mixed Variable Symplectic method` (`RMVS3`, Levison and Duncan, 1994) from the `swift`[1] package. The original code was extended to include the Yarkovsky effect (Nesvorný and Vokrouhlický, 2006). Each of the cluster members was represented by 200 to 300 orbital clones for this test. Due to the high number of possible combinations of clones (i.e., 200^N for N asteroids each represented by 200 clones), we limited the ΔV computation to tens or hundreds of thousands combinations at each output time, which was 4 years (except for the cluster of Nicandra, where the output time was 200 days). For each of the eight clusters (see Pravec et al., 2018, *Supplementary Information*) we obtained a sufficient number of convergences with reasonable shape (single dominant peak in most cases) of their time distribution. In two cases with many recorded convergences, clusters of Kap'bos and Nicandra, we also put a constrain for a mean anomaly dispersion $|\Delta M| < 90^\circ$ (ΔM is defined analogously to $\Delta\Omega$ and $\Delta\varpi$ in Equation 2.14). This helped us filter the most trustworthy convergences (since this method does not take into account the relative positions of the clones).

To confirm the membership of each member of a given cluster, we performed another backward orbital integrations for 11 of the 13 cluster. We omitted the

[1] Available at https://www.boulder.swri.edu/~hal/swift.html

clusters of Datura and Schulhof, since similar procedure was recently applied to them in Vokrouhlický et al. (2016, 2017). The goal of these integrations was to detect slow and close encounters between the orbital clones of a primary and each of the secondaries (more information about this method is described in Section 2.2.3). We used 500 orbital clones for each asteroid and we checked all 500×500 clone combinations for each primary-secondary pair every 200 days.

Comparison with the rotational fission theory

For each of the 13 clusters, we calculated the mass ratio q for of the total mass of all secondaries and the primary as

$$q \equiv \sum_{j=2}^{N} q_j \equiv \frac{\sum_{j=2}^{N} M_j}{M1}, \tag{3.1}$$

where q_j is a mass ratio of jth component of the cluster ($j = 1$ for primary and $j > 1$ for secondaries), N is the total number of confirmed cluster members and M_j is a mass of jth component. Assuming a same geometric albedo and a same bulk density for all cluster members, we estimated the mass ratio q_j as

$$q_j = 10^{-0.6(H_j - H_1)}, \tag{3.2}$$

where H_j is the absolute magnitude of jth component and H_1 is the absolute magnitude of the cluster primary. Combining the two previous equations, we could simply calculate the equivalent absolute magnitude of all the secondaries H_{seceq} in a given cluster as

$$q = 10^{-0.6(H_{\mathrm{seceq}} - H_1)} \quad \rightarrow \quad H_{\mathrm{seceq}} = H_1 - \frac{5}{3} \log_{10} q. \tag{3.3}$$

Once we derived H_{seceq} values for all the studied clusters, we calculated the differences of absolute magnitudes between a primary and all the secondaries $\Delta H \equiv H_{\mathrm{seceq}} - H_1$. With a known rotational period of cluster primaries P_1 and calculated ΔH, we compared these values against predictions from the theory of rotational fission of a rubble-pile asteroid proposed in Scheeres (2002, 2007) and applied by Pravec et al. (2010). We obtained an excellent agreements for 11 asteroid clusters, see Figure 3.1. Both outliers, clusters of Hobson and Mandragora, are shifted towards lower ΔH values (higher mass ratio), while the observed rotational periods of the two primaries are common. Looking at Figure 3.1, it is apparent that there are no obvious differences between asteroid pairs and clusters in the P_1 vs. ΔH distribution and therefore the theory of a rotational fission seems to successfully describe the formation mechanism for most of the asteroid pairs, but is also applicable for a majority of the asteroid clusters.

Interesting asteroid clusters

In the following few sections, we point out and further comment some of the interesting results obtained for selected asteroid clusters. We also mention a few updates for some of the clusters. See Pravec et al. (2018) for complete results for each of the studied clusters.

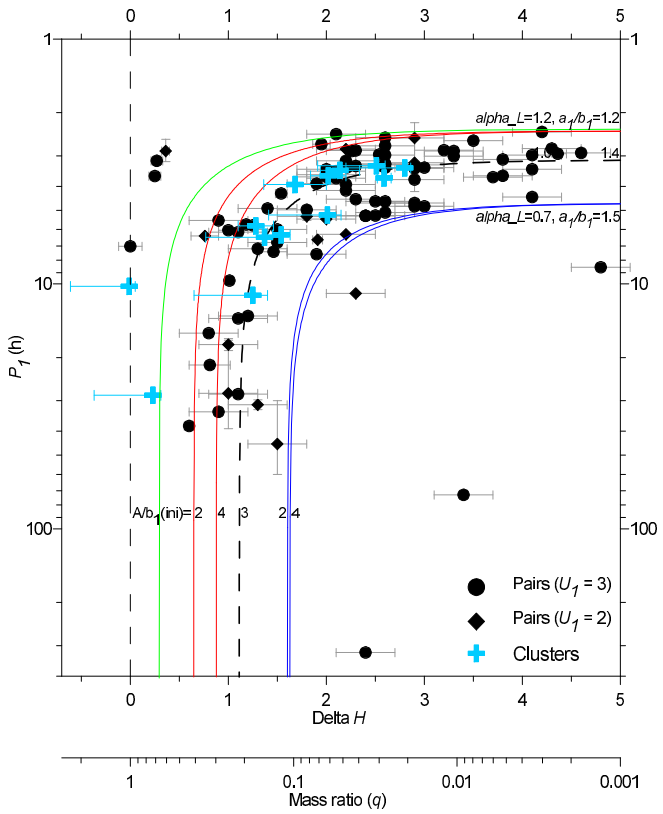

Figure 3.1: Most of the asteroid clusters (11/13; blue crosses) are consistent with the rotational fission theory of a rubble pile asteroid (solid lines). Asteroid pairs are labeled with black symbols. Figure taken from Pravec et al. (2018).

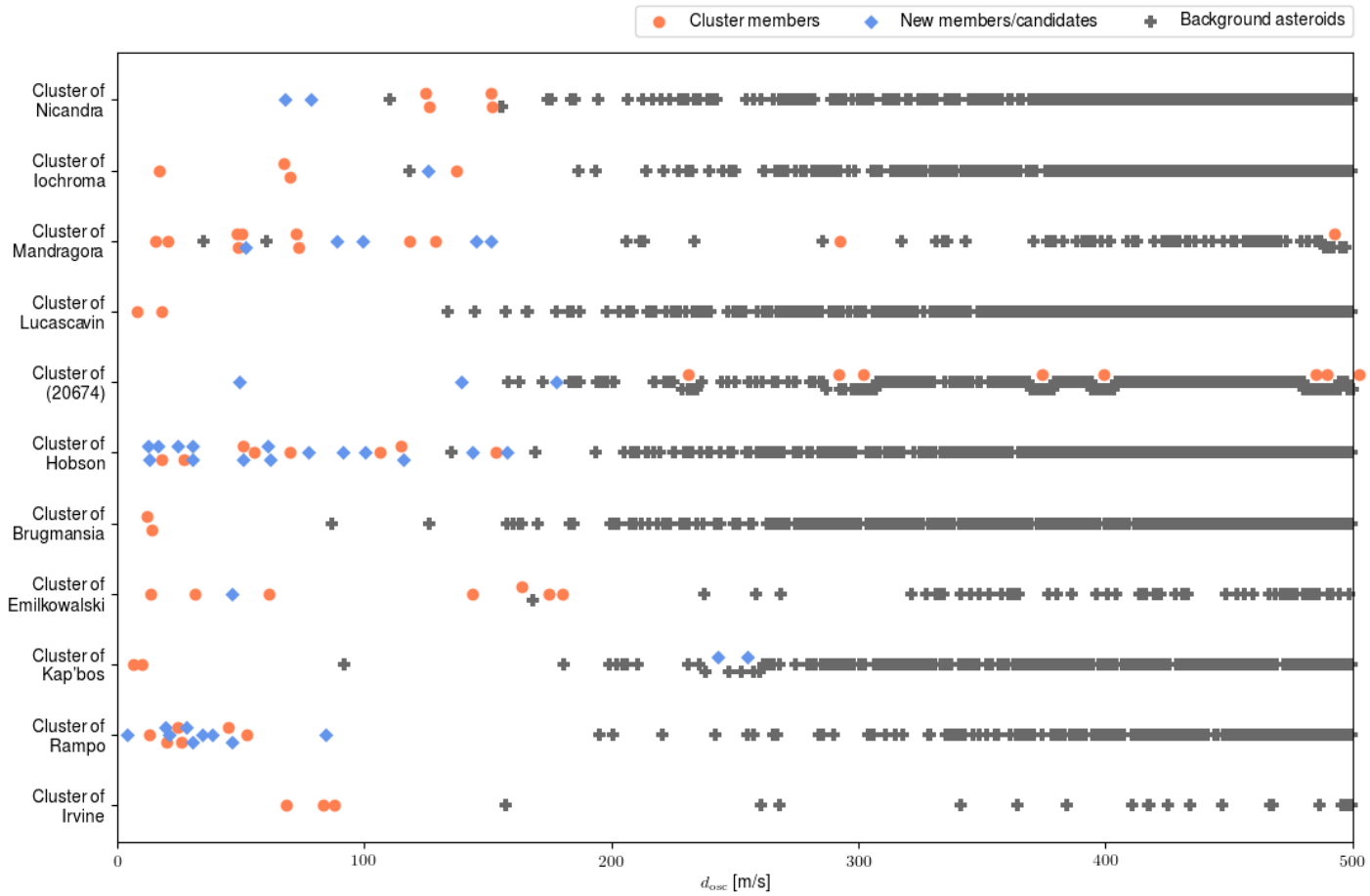

Figure 3.2: The distribution of d_{osc} distances of asteroids around the primaries of the eleven studied clusters in the osculating orbital elements. Confirmed members are represented by orange circles, new candidates by blue rhombuses and background asteroids by grey crosses. Small offsets along the y axis were applied to some points, where the cluster members' markers overlapped with other asteroid markers.

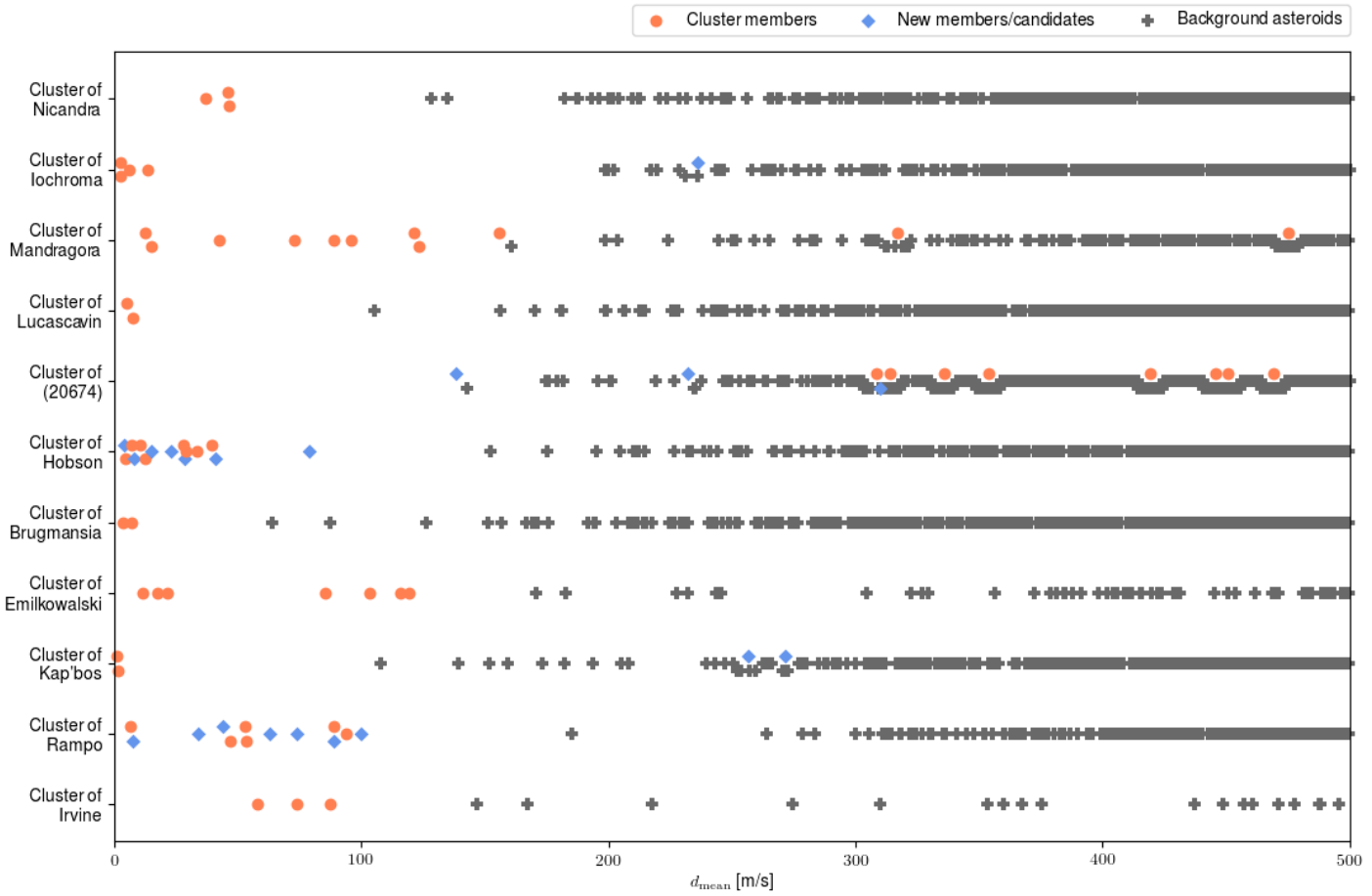

Figure 3.3: The distribution of d_{mean} distances of asteroids around the primaries of the eleven studied clusters in the osculating orbital elements. Confirmed members are represented by orange circles, new candidates by blue rhombuses and background asteroids by grey crosses. Single-opposition asteroids are not included, since the mean orbital elements are not computed for them by the `AstDyS-2` service. Small offsets along the y axis were applied to some points, where the cluster members' markers overlapped with other asteroid markers.

Cluster of (10321) Rampo

The asteroid (10321) Rampo is an probable S type asteroid with derived absolute magnitude $H_1 = 14.60 \pm 0.09$, effective diameter of 3.8 km, rotational period $P_1 = 5.2282 \pm 0.0007$ h and lightcurve amplitude of 0.69 mag (all from Pravec et al. (2018), where more details can be found). For the known seven members of this cluster (including the primary), Pravec et al. (2018) derived $q = 0.062$. Since the publication of this paper, we have found nine new candidate members (see Table 3.1 and Figures 3.2 and 3.3) of this cluster. These new probable members were identified in the space of osculating or mean orbital elements, in which they are at distances from the primary $d_{\mathrm{osc/mean}}$ comparable with the previously confirmed members. We also tested convergences of secular angles Ω and ϖ by integrating Yarkovsky clones (see Section 2.2.1 for method description). We confirmed that the secular angles of each new secondary converge with the secular angles of the primary at times around 700 kyr with one exception; asteroid 2015 TA367 is the closest asteroid to the primary in space of osculating orbital elements with $d_{\mathrm{osc}} = 3.9$ m/s and the second closest one in the space of mean orbital elements with $d_{\mathrm{mean}} = 7.4$ m/s. Its current secular angles are very similar to the primary's with $\Delta\Omega \approx 0.62^\circ$ and $\Delta\varpi \approx 0.25^\circ$ and a suggested age by the performed test for this secondary is anytime from the present up to ~ 1.2 Myr in the past (this is due to the limitations of the performed test for initially very similar orbits).

Taking all the new secondaries into account, the recalculated $q = 0.10$ (or $H_{\mathrm{seceq}} = 16.25$, $\Delta H = 1.65$), which is larger by 65% than the previously estimated value, but it is still within predicted values by the theory of rotational fission. In fact, in Figure 3.1 the recalculated value of q would put the cluster of Rampo significantly closer to the dashed line (representing the best set of parameters for asteroid pairs and clusters, for more details see Section 5 in Pravec et al., 2018), along which the rest of the clusters are aligned (with the exception of two outliers - clusters of Hobson and Mandragora, see discussion in following sections).

Cluster of (14627) Emilkowalski

The primary (14627) Emilkowalski of this cluster is an asteroid with estimated $H = 13.61 \pm 0.06$ and derived diameter of 6.9 km (with refined geometric albedo $p_v = 0.13$). Its rotational period is $P_1 = 11.1313 \pm 0.0009$ and the observed lightcurve amplitude is 0.67 mag. According to Vereš et al. (2015) and measured $(V - R)$ color index by Pravec et al. (2018), Emilkowalski is a relatively rare D-type asteroid. We note that the derived geometric albedo is not in an agreement with a typical geometric albedo for D-type asteroids (Burbine, 2016), but it is higher by a factor of several.

Before the work of Pravec et al. (2018), only four members of the Emilkowalski cluster were known. Apart from the primary, they were (126761), (256124) and (224559). Nesvorný and Vokrouhlický (2006) estimated the age of this cluster[2] to be 220 ± 30 kyr, but they noted that the convergence of secular angles for (126761) was not perfect. The previously estimated young age of this cluster is

[2]Only secondaries (126761) and (224559) were associated with this cluster at that time. Secondary (256124) was discovered later and was used to confirm the previously estimated age of this cluster.

Table 3.1: Members and candidate members of the asteroid cluster of (10321) Rampo with their absolute magnitudes H, distances $d_{\mathrm{osc/mean}}$ to the primary from the primary. In brackets is the ordinal number of given asteroid ordered by the distance from the primary in given orbital elements.

Asteroid		H [mag]	d_{osc} [m/s]	d_{mean} [m/s]	Status
(10321)	Rampo	14.60 ± 0.09^{a}	-	-	primary
(294272)	2007 UM101	17.5	13.0 (2.)	6.4 (1.)	member
(451686)	2013 BR67	17.8	45.1 (12.)	88.7 (10.)	member
	2016 TE87	18.0	26.0 (7.)	46.8 (5.)	member
	2009 HD95	18.1	30.3 (9.)	-	candidate
	2015 HT91	18.1	52.4 (14.)	93.7 (12.)	member
	2006 UA169	18.2	19.7 (4.)	52.6 (6.)	member
	2017 UH21	18.3	34.1 (10.)	73.7 (9.)	candidate
	2014 HS9	18.4	24.3 (6.)	53.3 (7.)	member
	2013 RL101	18.4	38.3 (11.)	88.9 (11.)	candidate
	2015 TM372	18.5	20.7 (5.)	44.1 (4.)	candidate
	2013 VC30	18.5	27.6 (8.)	62.6 (8.)	candidate
	2010 VO19	18.6	46.2 (13.)	99.9 (13.)	candidate
	2009 SR371	18.7	19.6 (3.)	33.9 (3.)	candidate
	2015 TA367	18.8	3.9 (1.)	7.4 (2.)	candidate
	2014 HN87*	18.8	84.2 (15.)	-	candidate

*Single-opposition asteroids.

[a]From Pravec et al. (2018). The remaining H values were taken from the `AstDyS-2` database (downloaded December 8, 2019).

Table 3.2: Members and candidate members of the asteroid cluster of (14627) Emilkowalski with their absolute magnitudes H, distances $d_{\mathrm{osc/mean}}$ to the primary from the primary. In brackets is the ordinal number of given asteroid ordered by the distance from the primary in given orbital elements.

Asteroid		H [mag]	d_{osc} [m/s]	d_{mean} [m/s]	Status
(14627)	Emilkowalski	13.61 ± 0.06^a	-	-	primary
(126761)	2002 DW10	15.3	61.4 (4.)	21.4 (3.)	member
(256124)	2006 UK337	15.9	13.4 (1.)	17.2 (2.)	member
(224559)	2005 WU178	16.7	31.5 (2.)	11.3 (1.)	member
(434002)	2000 SM320	16.9	174.6 (8.)	119.4 (7.)	member
	2014 UV143	17.5	143.6 (5.)	103.2 (5.)	member
	2009 VF107	17.6	163.8 (6.)	85.5 (4.)	member
(476673)	2008 TN44	17.8	180.1 (9.)	115.7 (6.)	member
	2018 VB69*	18.0	46.3 (3.)	-	candidate

*Single-opposition asteroid.

[a]From Pravec et al. (2018). The remaining H values are taken from the `AstDyS-2` database (downloaded December 8, 2019).

supported by the association with a young, still forming, dust band located at $\sim 17^\circ$ ecliptic latitude (e.g., Vokrouhlický et al., 2008b; Espy Kehoe et al., 2015). However, we found and verified the membership of three new asteroids belonging into this cluster, which are (434002), 2014 UV143 and (476673). Interestingly, our integration results for any of these new members are not in an agreement with the previously estimated age of this cluster. In fact, the earliest recorded slow encounters for the newly identified members appear at time $\sim$ 1 700 kyr and their estimated ages (median of all clone encounters) are 2 258, 3 100 and 3 447 kyr for (434002), 2014 UV143 and (476673), respectively. These ages for the new members are much higher and the time distributions of close and slow encounters have a little or no overlap with two young members (256124) and (224559). All three of these new members are with $d_{\mathrm{mean}} > 100$ m/s relatively far from the primary and also from the rest of the cluster, but they are remarkably close to each other with mutual $d_{\mathrm{mean}} \leq 18$ m/s. The possibility of a "cascade fission", when a parent asteroids underwent multiple break-ups at significantly different times, was very intriguing for us and become the motivation for our later study (see Fatka et al., 2020), where we searched for more asteroid cluster suggesting multiple break-up events in their recent history, similarly as the cluster of Emilkowalski.

In Fatka et al. (2020) we have discovered a new probable, but still single-opposition, member of this cluster - asteroid 2018 VB69. It is the third closest asteroid to the primary (see Figure 3.2), but due to its small size (resp. large absolute magnitude $H = 18.0$ mag) the mass ratio q increases only by 2.4×10^{-3}. Therefore, the position of this cluster does not change notably in Figure 3.1.

Cluster of (18777) Hobson

The primary asteroid of this cluster (18777) Hobson is a probable S type asteroid with $H = 15.16 \pm 0.05$, lightcurve amplitude 0.21 mag, rotational period $P_1 = 10.227 \pm 0.004$ h and estimated 3 km diameter (assuming the geometric albedo 0.2, which is the mean geometric albedo for S type asteroids Pravec et al., 2012).

We performed an orbital integration searching for close and slow clone encounters between eight multi-opposition secondaries and the primary (we omitted two single-oppositional member candidates due to the large uncertainty in their orbit estimations). The time distributions of recorded encounters nicely overlap for all eight secondaries and suggest that this cluster formed about 350 kyr ago, which is in an agreement with estimated age 365 ± 67 kyr by Rosaev and Plávalová (2017). We obtained a rather small number of clone encounters between the smallest secondary 2014 HH103 and the primary. We suspect this was because of the large uncertainty of orbital elements, large range of possible Yarkovsky drift strength for a such small body and the limited number of clones used.

Interestingly, the calculated mass ratio for this cluster was $q = 1.014$, which means that more mass is stored in the escaped secondaries than in the remaining primary. This finding was in a strong disagreement with a predicted upper limit $q \leq 0.2$ by the theory of rotational fission Pravec et al. (2010). We note that a recalculated mass ratio with updated catalog absolute magnitudes is $q = 0.957$. Moreover, since Pravec et al. (2018), we have found 15 new probable members of the Hobson cluster with catalog absolute magnitudes ranging from 17.4 to 19.0 (see table 3.3 and Figures 3.2 and 3.3). These new secondaries increase the mass ratio by ~ 0.28 to a new value $q = 1.237$. It is apparent that this cluster was not formed solely by a rotational fission, if at all. This cluster can be a product of a catastrophic collision, like many other asteroid families. If so, this would be one of the youngest asteroid families known today.

Table 3.3: Members and candidate members of the asteroid cluster of (18777) Hobson with their absolute magnitudes H, distances $d_{\mathrm{osc/mean}}$ to the primary from the primary. In brackets is the ordinal number of given asteroid ordered by the distance from the primary in given orbital elements.

Asteroid		H [mag]	d_{osc} [m/s]	d_{mean} [m/s]	Status
(18777)	Hobson	15.16 ± 0.05^a	-	-	primary
(57738)	2001 UZ160	15.41 ± 0.05^a	106.4 (18.)	4.2 (2.)	member
(436620)	2011 LF12	17.3	27.1 (6.)	6.7 (3.)	member
(363118)	2001 NH14	17.3	153.0 (23.)	27.7 (9.)	member
	2007 HC54	17.4	50.9 (10.)	-	candidate
	2007 EH116	17.6	12.3 (1.)	-	candidate
(537249)	2015 HM190	17.6	61.0 (12.)	28.5 (10.)	candidate
(450571)	2006 JH35	17.7	18.1 (4.)	33.3 (12.)	member
(381414)	2008 JK37	17.7	115.0 (19.)	10.2 (5.)	member
	2015 FV225	17.8	61.9 (13.)	-	candidate
(465404)	2008 HQ46	17.8	69.8 (14.)	39.5 (13.)	member
	2015 XL282	17.8	91.1 (16.)	40.6 (14.)	candidate
	2014 KY102	18.0	100.5 (17.)	-	candidate
	2014 HH103	18.1	50.8 (9.)	12.6 (6.)	member
(520394)	2014 JJ10	18.1	55.4 (11.)	28.9 (11.)	member
	2015 KA91	18.2	13.1 (2.)	22.8 (8.)	candidate
	2016 GY256*	18.2	24.2 (5.)	-	candidate
	2015 OP104	18.3	16.2 (3.)	14.9 (7.)	candidate
	2014 NN71	18.3	157.7 (24.)	7.9 (4.)	candidate
	2017 SQ83	18.4	115.7 (20.)	3.9 (1.)	candidate
	2014 OG277*	18.6	77.1 (15.)	79.0 (15.)	candidate
	2015 PM156	18.8	30.3 (7.)	-	candidate
	2014 OJ66*	18.9	143.8 (22.)	-	candidate
	2015 HV138	19.0	30.6 (8.)	-	candidate

*Single-opposition asteroids.

[a]From Pravec et al. (2018). The remaining H values are taken from the `AstDyS-2` database (downloaded December 8, 2019).

Cluster of (22280) Mandragora

Asteroid (22280) Mandragora is a 9.8 km sized primary of this cluster with $H = 14.02 \pm 0.07$, lightcurve amplitude 0.09 mag and probable rotational period $P_1 = 28.48 \pm 0.03$ h.

This cluster was one of the newly discovered one. At first two secondaries were identified as an significant pair and later two more asteroids, including the primary, were associated with the pair. With relaxing d_{mean} limit around each member, six new candidates were found with d_{mean} up to 161 m/s from the primary, but all with $d_{\mathrm{mean}} < 100$ m/s from at least one other member. The increasing number of secondaries with similar H at higher distances prompted us to employ the hierarchical clustering method (HCM) that is typically used for identifying members of large and typically old asteroid families. With the HCM we identified another seven candidate members and finally two more candidates were found near one of the secondaries discovered by HCM. During work on another project (after publication of Pravec et al., 2018), we checked convergences of the secular angles (see section 2.2.2) of all asteroids around the primary up to distance $d_{\mathrm{osc}} \leq 200$ m/s and we identified five new, single-opposition candidate members of this cluster (see Table 3.4 and Figure 3.4). We note that this procedure (used to identify the five new candidates) is not reasonably applicable at high distances from the primary due to the high density of orbits around it. A different approach, such as HCM, is required for finding new possible members of this cluster. We leave this search for possible future study.

We performed backward orbital integrations searching for close and slow encounters for all the 18 multi-opposition member candidates and verified their membership. For all of the secondaries we recorded clone encounters between times 100 and 400 kyr ago and in several cases, the time distribution of encounters had tails reaching up to 1 Myr, where our integrations ended (see Fig. 10 and 11 in Pravec et al., 2018). From six time distributions with at least 500 recorded encounters, we estimated the age of this cluster to be 250^{+290}_{-90} kyr. The test of secular angle convergence reveled that all of the new five single-opposition member candidates show separation event at time consistent with estimated age of this cluster. An updated mass ratio with new candidate members included is $q = 0.739$ (without new members and with updated H values, $q = 0.694$). This new value of q shifts this cluster even further away from the limits predicted by the theory of a rotational fission. Also it is highly probable that there are more, not yet associated or discovered, asteroids belonging into this cluster. Therefore, it can be expected that the mass ratio will increase even further once they are identified.

We obtained mutually consistent age estimations for secondaries close to the primary with $d_{\mathrm{mean}} < 36$ m/s as well as for secondaries with distances $d_{\mathrm{mean}} > 2\ 000$ m/s from the primary (see Table 1 and Figures 11 and 12 in Pravec et al., 2018). These extremely large differences of distances in the space of mean orbital elements among members of a single cluster is highly unusual. A probable explanation could be the fact that this cluster is located near a mean motion resonance J9/4 with Jupiter, which could cause large displacements in the space of osculating and mean orbital elements for some of the cluster members. This would also explain a smaller number of recorded encounters for the more distant secondaries if we compare them with the close members. Also the current

rotational period of the primary is slower by a factor of few than any other cluster primary. Similarly as the cluster of Hobson, the cluster of Mandragora could not be formed solely by a rotational fission of a rubble pile parent asteroid. Another formation mechanism, such as a catastrophic collision, must be responsible for its formation.

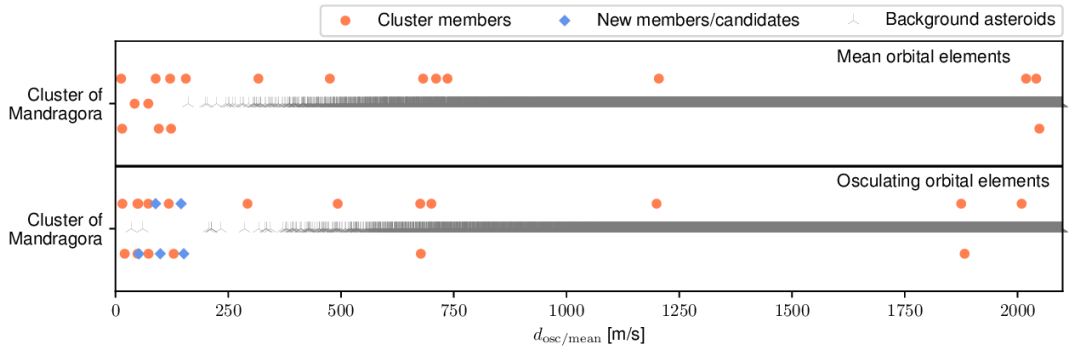

Figure 3.4: The distribution of $d_{\mathrm{osc/mean}}$ distances of asteroids around the primaries of both osculating and mean orbital elements with distances up to 2 100 m/s. Confirmed members are represented by orange circles, new candidates by blue rhombuses and background asteroids by grey symbols. Single-opposition asteroids are not included for the distribution in mean orbital elements, since they are not computed for them by the `AstDyS-2` service. Small offsets along the y axis were applied to some points, where the cluster members' markers overlapped with other asteroid markers.

Table 3.4: Members and candidate members of the asteroid cluster of (22280) Mandragora with their absolute magnitudes H, distances $d_{\mathrm{osc/mean}}$ to the primary from the primary. In brackets is the ordinal number of given asteroid ordered by the distance from the primary in given orbital elements.

Asteroid		H [mag]	d_{osc} [m/s]		d_{mean} [m/s]		Status
(22280)	Mandragora	14.02 ± 0.07^a	-		-		primary
(43239)	2000 AK238	14.90 ± 0.04^a	675.7	(433.)	710.7	(1352.)	member
(204960)	4713 P-L	16.2	1882.7	(16495.)	2041.5	(26529.)	member
(265395)	2004 TM4	16.4	1875.1	(16368.)	2048.5	(26733.)	member
(324154)	2005 YN176	16.5	15.2	(1.)	14.7	(2.)	member
(284995)	2010 KF124	16.5	48.8	(5.)	121.0	(7.)	member
(180105)	2003 FB12	16.5	50.4	(6.)	95.8	(6.)	member
(296045)	2009 AX18	16.6	128.9	(14.)	123.1	(8.)	member
(327558)	2006 CE52	16.6	292.6	(23.)	316.7	(30.)	member
(391017)	2005 SX208	16.6	1199.7	(5151.)	1204.7	(8395.)	member
(472944)	2015 GH28	16.7	118.1	(13.)	72.7	(4.)	member
	2011 LT11*	16.8	151.4	(16.)		-	candidate
(412122)	2013 GQ30	16.8	492.6	(90.)	475.2	(159.)	member
(446436)	2014 JY39	16.9	48.6	(4.)	155.8	(9.)	member
(459310)	2012 GZ32	17.1	20.3	(2.)	12.5	(1.)	member
(513829)	2013 EC88	17.1	73.1	(10.)	89.0	(5.)	member
	2008 HP40	17.2	700.3	(520.)	682.0	(1097.)	member
(373667)	2002 QX88	17.3	676.9	(437.)	736.1	(1583.)	member
	2014 OO240*	17.4	99.2	(12.)		-	candidate
(514734)	2007 BJ41	17.5	72.5	(9.)	42.3	(3.)	member
	2012 FA11*	17.6	51.7	(7.)		-	candidate
	2007 DQ110*	17.9	145.4	(15.)		-	candidate
(490713)	2010 RY26	18.1	2009.2	(19196.)	2018.9	(25849.)	member
	2015 BF423*	18.3	88.8	(11.)		-	candidate

*Single-opposition asteroids.

[a]From Pravec et al. (2018). The remaining H values are taken from the `AstDyS-2` database (downloaded December 8, 2019).

3.2 Asteroid pairs: A complex picture

The number of known asteroid pairs is currently counted in hundreds and the amount of available data for them has grown in the last few years significantly. In Pravec et al. (2019) we chose asteroid pairs for which we could reliably derive (from photometric observations) the rotational period of the primary component. We obtained and further studied a sample of 93 pairs. For the 93 chosen pairs, we performed backward orbital integrations and we estimated a separation time of the two pair components (the age). We tested the asteroid pairs data against the prediction of the theory of rotational fission of a ruble-pile parent asteroid (Pravec et al., 2010) and we found a good agreement for 86 of 93 studied pairs. Interestingly, in 13 cases, the primary asteroids of given pairs are in fact a systems of two or three components - binary or triple systems. These systems consist of one significantly larger component and one or two smaller components (satellites) orbiting around the large one. We also performed a taxonomy assignment based on photometric colors for several dozen asteroids. For 19 asteroids, we determined their pole position. In both cases, in which we had estimations for both the primary and the secondary, we obtained the same sense of rotation and we also constrained the angles between their original spin vectors at the time of their separation. As a byproduct, we discovered three new asteroid cluster and estimated their age.

Backward orbital integrations

Unlike in our previous work (Pravec et al., 2018), we substituted the `RMVS3` integrator from the `swift` package by an implementation of symplectic Wisdom-Holman integrator `WHFast` (Rein and Tamayo, 2015) included in the `REBOUND` package (Rein and Liu, 2012). This transition allowed us to include more orbital clones of studied asteroids (see Section 2.2.3) in our backward orbital integrations. This increase meant that we sampled a larger area of the initial orbit uncertainty hyper-ellipsoid of each asteroid and also that we sampled more possible strengths of the Yarkovsky drift, which is especially important for secondaries, which are more influenced by the Yarkovsky effect than primaries due to their smaller sizes. Because of the native support of parallel computing in `REBOUND`, we were able to shorten the integration time-step to only a few hours and to significantly increase the frequency of encounter checks between clones, while keeping the computational time reasonably short (within a few days). The shorten time-step improves an overall stability and reliability of integrations. A higher frequency of clone encounter checks increases the probability of finding two clones at smaller distances and lower relative velocities during an encounter simply due to the higher sampling rate. The last difference from integrations performed in Pravec et al. (2018) are the mass particles included. In Pravec et al. (2018) we computed the gravitational attraction of the Sun and all the eight major planets, whereas in this work, we added the gravitational attraction of two dwarf planets Pluto and Ceres and two large asteroids Vesta and Pallas. We notices that encounters between asteroids' orbital clones and the Main Belt objects Ceres, Vesta or Pallas are relatively common in our simulations, meaning that the inclusion of these large objects in our simulations better represented the true orbital evolution of studied

asteroids.

Primary's rotation vs. mass ratio relation

For the studied sample of 93 asteroid pairs, 86 (over 92%) of them falls within the limits set by the theory of rotational fission of a rubble-pile parent asteroid. Unlike asteroid clusters (see Figure 3.1), in Figure 3.5 asteroid pairs are more scattered along the dashed line representing the "best" set of parameters used in the model of rotational fission. However, we must note that the sample of known asteroid pairs is much richer by a factor of ∼8 than the sample of asteroid clusters.

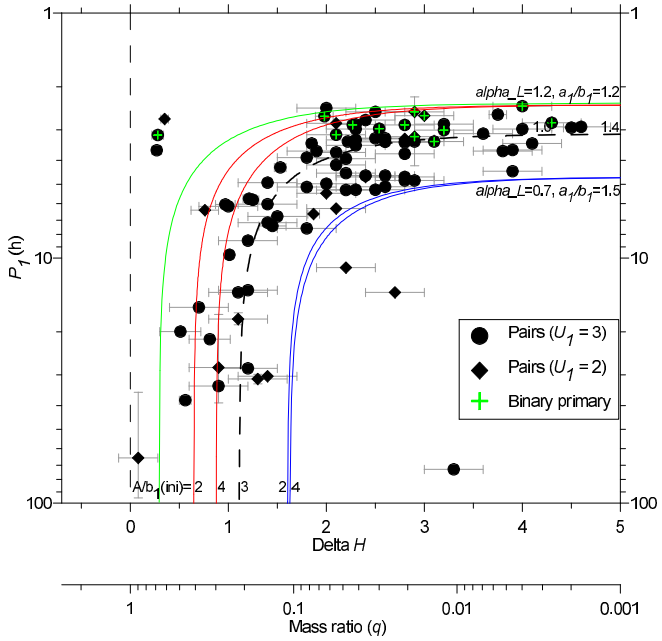

Figure 3.5: Primary rotation periods vs mass ratios of asteroid pairs with highlighted pairs whose primary is a binary (or tertiary) asteroid (green crosses).

The primaries of three out of the seven outliers rotate too slowly and are located below the established lower limit. It is unlikely that the rotational periods of primaries are in error by several hours, especially for the pair (53537)–(503955), where the primary's rotational period would have to be at least 14× shorted than the measured period. But in principle, wrongly estimated rotational period cannot be ruled out. Another explanation for these three outliers is that they are not asteroid pairs, but asteroid clusters and we did not find rest of it. If new members were found, the mass ratio q would be larger (ΔH would be smaller) and the clusters' mass ratios would shift towards the predicted values for a given rotational period of the primary. The shift would off course depend on the total mass of newly discovered members. We explored[3] the surrounding in the space of osculating (with single-opposition asteroids included) and mean orbital elements

[3]We performed the test of secular angles convergences for all asteroids with $d_{\mathrm{osc/mean}} \leq 200$ m/s (see section 2.2.2) followed by backward orbital integration for selected candidates (see section 2.2.3).

around these three asteroid pairs to distances up to 200 m/s (which is at least 11× larger distance than d_{mean} for given pairs), but we did not find any candidate members. We plan to perform additional tests to check whether hypothetical members of these pairs could be found at higher distances from them.

The remaining four asteroid pairs, not following the predicted trend, have too high mass ratio. To "correct" these outliers, we would have to find a new primary asteroids of these pairs/clusters. For each the four outliers, we checked the secular angles convergence for 70 closest asteroids with their absolute magnitudes $H \leq H_{\mathrm{primary}} + 0.5$. We checked only asteroids larger than the primary in a given cluster, but we relaxed the H criterion by 0.5 mag to account for uncertainties of H estimation in catalog. We did not find any suitable candidate for any of the four pairs. Three outliers located close to each other in the top left corner in Figure 3.5 are young pairs with estimated ages 141, 143 and 250 kyr and according to `AstDyS-2` website, their orbits are stable for at least a several hundred thousands years. Therefore it is unlikely that their hypothetical primaries would have enough time to drift far away from the known pairs in the space of orbital elements. An explanation in the form of another formation mechanism might be needed to describe the origin of these high mass ratio pairs. Also, this new explanation needs to account for the fact that one primary of these four outlying pairs, asteroid (80218), is in fact a binary asteroid with a bound, synchronous satellite.

Binary asteroids among asteroid pairs

Among the 93 studied asteroid pairs, we have found that 13 primaries have a bound satellite orbiting around them. In one case, pair (3749)–(312497), a second satellite was discovered. Another five primaries of studied pairs are considered binaries candidates (see '?' in column 'Sat.$_1$' in Table 1 in Pravec et al., 2019), but confirmation with more data is needed. If we also consider that our detection methods are not perfect, the real amount of binary systems among asteroid pairs can be much higher. We predicted taht there is at least 50% binaries among the fastest rotating primaries of asteroid pairs. Interestingly, primaries of these 13 recognised pairs are all fast rotators with rotational periods ≤ 3.35 h (see green crosses in Figure 3.5). These binaries also share some common features with many binaries among known near-Earth and small main belt binary asteroids, i.e., the primaries are relatively spherical or that the bound secondaries are relatively small with $D_{\mathrm{sec}}/D_{\mathrm{prim}} < 0.5$ (for more information see Section 5.1 in Pravec et al., 2019).

A possible explanation of an origin of an asteroid pair with binary primary was proposed by Jacobson and Scheeres (2011) as a possible outcome of a secondary fission process. The secondary fission happens when a secondary asteroid of a binary system is rotationally accelerated via gravitational torques until it undergoes a fission and creates a chaotic ternary system. Further evolution of the chaotic ternary system has several different final forms, but one of them is when one secondary escaped and one remains bound (on a stable orbit) to the primary. However, this theory does not explain why the primary components should be fast rotators, as this preference can be clearly seen in Figure 3.5. Another possible explanation is that a primary underwent two rotational fission at different times.

The result of the first one (that happened further in the past) was a formation of a secondary orbiting on a stable orbit. The rotation of the primary was slowed down by the separation of the secondary. Then, the primary was spun up by the YORP effect to its critical rotation again and underwent another rotational fission resulting in a formation of another secondary. The newly formed secondary gravitationally interacted with the primary as well with the older secondary and broke the orbital stability of the system. One of the possible results could be an escape of one of the secondary, while the other one stabilized its orbit around the primary. This hypothesis of cascade fission of a primary component was proposed in Pravec et al. (2018) for the asteroid cluster of Emilkowalski and further studied in Fatka et al. (2020).

Interesting cases

Asteroid pair (3749) Balam – (312497) 2009 BR60

The asteroid system (3749) Balam is very interesting, because (apart of being a member of an asteroid pair) it consist of three bodies - one dominant (primary) and two small satellites (bound secondaries) orbiting around it. The primary is a 4.1 km sized (mean diameter) asteroid and the unbound (escaped) secondary is a small $\sim$ 650m asteroid. The larger bound secondary is a relatively large object with a mean diameter 1.9 km and it is orbiting at distance of only $\sim$ 13 km from the primary's center of mass. It also appears that its rotational period is same as its orbital period (it is in s synchronous spin state). Its orbit is slightly eccentric with eccentricity ranging from 0.03 to 0.08 (estimated 3σ interval). The smaller bound secondary is a 1 km sized object, whose orbit is unusually eccentric with eccentricity being somewhere between 0.3 and 0.8 and with semi-major axis being around 225 km. More information about discovery history, parameters derivation, etc., can be find in Pravec et al. (2019) and references herein.

Cluster of (157123) 2004 NW5

We discovered three new asteroid clusters during our search for asteroid pairs. All of them consist of three members and for the clusters of (5478) Warburg and (10484) Hecht, our backward orbital integrations suggest a single separation time for both secondaries of each cluster (for more information see Appendix C in Pravec et al., 2019). Interestingly, for the cluster of (157123) 2004 NW5, the time distributions of clone encounters between the primary and secondaries are significantly different. The median values of their clone encounter times are 146 kyr for secondary 2002 QM97 and 1 786 kyr for secondary (385728) 2005 UG350, which is a difference of more than 1.6 Myr. The number of clone encounters for the older secondary is low and they are scattered over the range of 1.5 Myr, which is probably caused by the location of the cluster in a dynamically chaotic zone. With the measured rotational period 3.588 ± 0.0005 h of the primary and calculated mass ratio 0.447 (for definition see 3.3), this cluster is located just beyond the limits predicted by rotational fission (see Figure 3.5). Therefore, we also considered that asteroid (157123) is not the real primary of this cluster, but we did not find any suitable candidate in the proximity of this cluster. It is

possible that it is more distant from the rest of the cluster due to the high orbital chaoticity. This is a second cluster[4], in which we suspect two or more separation events that happened at significantly different times. We performed further study of this cluster in Fatka et al. (2020).

3.3 A common origin for dynamically associated near-Earth asteroid pairs

As we already know, there are hundreds of known asteroid pairs and dozens of asteroid cluster in the asteroid Main Belt, but there are only a few probable asteroid pairs or clusters in the near-Earth asteroid population. We performed a search for young asteroid pairs and performed backward orbital integrations for several candidates. We ended up with two probable asteroid pairs, whose orbits suggest a possible common origin. Another supporting fact for a these two pairs being real is that both components of each pair were assigned with the same taxonomic class.

Candidate selection and backward orbital integration

For the initial search of close orbits among near-Earth asteroids, we used the Lowell `astorb` database[5], which contained about 20 000 orbits for known near-Earth asteroids. We tested several different metrics with various number of orbital elements and we chose the dimensionless D-criterion revised by Drummond (1981)[6] defined as

$$D^2 = \left(\frac{e_1 - e_2}{e_1 + e_2}\right)^2 + \left(\frac{q_1 - q_2}{q_1 + q_2}\right)^2 + \left(\frac{I}{180^\circ}\right)^2 + \left(\frac{e_1 + e_2}{2}\frac{\Theta}{180^\circ}\right)^2, \tag{3.4}$$

where q_1 and q_2 are perihelion distances and I and Θ are defined as

$$I = \arccos\left[\cos i_1 \cos i_2 + \sin i_1 \sin i_2 \cos\left(\Omega_1 - \Omega_2\right)\right], \tag{3.5}$$

$$\Theta = \arccos\left[\sin \beta_1 \sin \beta_2 + \cos \beta_1 \cos \beta_2 \cos\left(\lambda_1 - \lambda_2\right)\right], \tag{3.6}$$

where $\beta = \arcsin\left(\sin i \sin \omega\right)$ is ecliptic latitude of perihelion point and $\lambda = \Omega + \arctan\left(\cos i \tan \omega\right)$ is ecliptic longitude of perihelion point. Values of D range from 0, for two identical identical orbits, to $\sqrt{3.25} \approx 1.8$, for two most different elliptical orbits.

The use of backward orbital integration method is a bit more difficult for objects that may experience close encounters with massive bodies, such as planets. This is exactly the case of integrating near-Earth asteroids, because, as their definition suggests, their orbits are relatively close to the orbit of Earth, but they may also experience encounters with Venus or Mars. One of the main differences from the integrations performed in Pravec et al. (2018, 2019) is that we replaced

[4]Cluster of Emilkowalski was the first one to suggest multiple disruption events (Pravec et al., 2018).

[5]Available at: *https://asteroid.lowell.edu/main/astorb*.

[6]The first version of this metric was originally introduced by Southworth and Hawkins (1963).

the symplectic integrator, which uses a fixed timestep, with a non-symplectic integrator that uses adaptive time-stepping - `IAS15` (Rein and Spiegel, 2015)[7]. The `IAS15` integrator adjust the length of each time-step during an integration to solve correctly each encounter with a massive body. This allowed us to perform the backward orbital integrations in the less stable zone near planets, but it also prolonged the time needed for a simulation to finish.

To get up-to-date orbital solutions for studied asteroids, we used `JPL Small-Body Database Browser`[8] to get the latest orbital fit and corresponding covariance matrix. In this database, the orbital solutions with covariance matrices are calculated for the center of asteroid's observed arc-span, therefore the orbital elements are calculated for different epoch for each asteroid. We dealt with this complication by finding, which of the two asteroids of candidate pair has its orbital solution closest to the present, then we started the simulation at this epoch, added all the mass objects responsible for gravitational interaction (the Sun, the eight major planets, Pluto, Ceres, Vesta and Pallas) and we created orbital clones of the asteroid with orbital solution for that epoch. Then, we integrated this set of particles to the past, until the epoch of orbital solution for the second asteroid from the pair was reached. This was in a range of a few days up to one year. Then we created orbital clones for the second asteroid of the pair and started a full integration with encounter detection enabled.

Due to the generally weak orbital stability of near-Earth asteroids and also due to the fact that many near-Earth asteroids have orbits determined from a single opposition, we relaxed a requirement of physically close encounter of orbital clones and we satisfied with MOID and relative velocities of hypothetical asteroids at MOID configuration (see the last paragraph in section 2.2.3). We also limited the length of integration to only a few dozens of kyr in to the past. Every 15 years of integration time, we computed the MOID and relative velocity between orbital clones of the two asteroids. We found two candidates for a recent break-up, which are discussed individually below.

2015 EE7 - 2015 FP124

The primary asteroid of this potential asteroid pair - 2015 EE7 is a 170^{+60}_{-30} meter sized asteroid with $H = 20.2$ and geometric albedo $0.37^{+0.20}_{-0.17}$ (Trilling et al., 2016). The secondary 2015 FP124 with $H = 22.2$ is an ~ 80 meter asteroid (assuming the same geometric albedo). Both asteroids are classified as Apollo type near-Earth asteroids with perihelion distance ~ 1.003 AU and aphelion distance ~ 2.4 AU reaching into the inner part of the Main Belt. Orbits of both asteroids are quite eccentric with eccentricities just above 0.41 and inclined with inclination $\sim 27°$.

The D value (quantifying the similarity of two orbits) for this pair is 0.0037 and it is among the smallest in the `astorb` database (updated April 1, 2019), therefore these two asteroids become strong candidates for being an asteroid pair. Our backward integration revealed that none of the 1 000 orbital clones (500 for each asteroid) experienced an encounter with any of the mass objects included in our integration in the past 5 kyr that would significantly influence its

[7]The `IAS15` integrator is part of the `REBOUND` package.

[8]Available at *https://ssd.jpl.nasa.gov/sbdb.cgi*.

orbit. Unfortunately, the observed orbital arc of 2015 FP124 was only 15 days long, therefore its orbital solution has large uncertainties. The condition code, quantifying the orbital solution quality, was 8 (with 0 being good and 9 being highly uncertain). The primary's observed orbital arc is 118 days long and its condition code was 3. Due to the orbital uncertainties of the secondary, we were not able to estimate a unique age for this pair. In Figure 3.6 left, it can be seen that slow encounters with v_{rel} smaller than a few m/s are recorded as well as small MOID values of only a few hundred kilometers. We found a large number of encounters with relatively large MOID ($>$ 15 000 km) at times below 1 000 yrs, but we thing that this could be only a series of real physical encounters, not the separation events, of these two asteroids. We also see encounters with small v_{rel} at times from 2 to 4 kyr ago. Even though these encounters are at MOID distances larger than 10^3, we thing that they might be more representative of the real age of this pair. The scatter of orbital clones in the mean anomaly grows rapidly due to the initial uncertainties and our sample of 500 clones becomes insufficiently sparse. With current orbital solutions, it is possible for asteroids 2015 EE7 and 2015 FP124 to have mutual encounters at slow relative velocities within the last 5 kyr. But it is also evident that a refinement of their orbits, especially for 2015 FP124, is needed for further restriction of separation time of the secondary from the primary.

Spectroscopic observations of 2015 EE7 were obtained by 8.19 m telescope Gemini South with GMOS instrument[9]. Based on these spectroscopic data, 2015 EE7 was classified as an Sq asteroid with indication of low degrees of space weathering. Asteroid 2015 FP124 was spectroscopically observed by the Goodman Spectrograph mounted on the 4.1 m SOAR[10] Telescope. Quality of the data obtained for 2015 FP124 was lower than for the primary, but they still provided useful information and enabled taxonomic assignment. The secondary was classified as a Q-type asteroid. Even though the specific assigned taxonomic types are not the same, Sq and Q types, they are relatively similar, see Fig. 1 in Moskovitz et al. (2019), and both are part of the same taxonomic S-complex. Also the worse data quality for 2015 FP124 could play a role in the asteroid's taxonomic assignment, because if the uncertainties of both measurements are taken into accounts and both spectra are compared against each other, they are statistically indistinguishable. This was determined by fitting error weighted polynomials to the data and by comparing the coefficients of the fits. The resulting coefficients were indistinguishable at the 1-σ level. More details about observations, data reduction and data processing can be found in Sections 2 and 3 in Moskovitz et al. (2019).

2017 SN16 - 2018 RY7

Asteroid 2017 SN16 is a primary of this probable asteroid pairs with $H = 23.2$ and its estimated mean diameter is about 50 meters. The secondary of this pair, 2018 RY9, has $H = 24.5$ and its diameter is about 25 meters. Both are classified as Apollo type asteroids with perihelion distance 0.86 AU and aphelion distance 1.16 AU. The eccentricity of their orbits is $\sim$0.15 and inclination is about 13.4°.

[9]GMOS = Gemini Multi-Object Spectrograph.
[10]SOAR = Southern Astrophysical Research

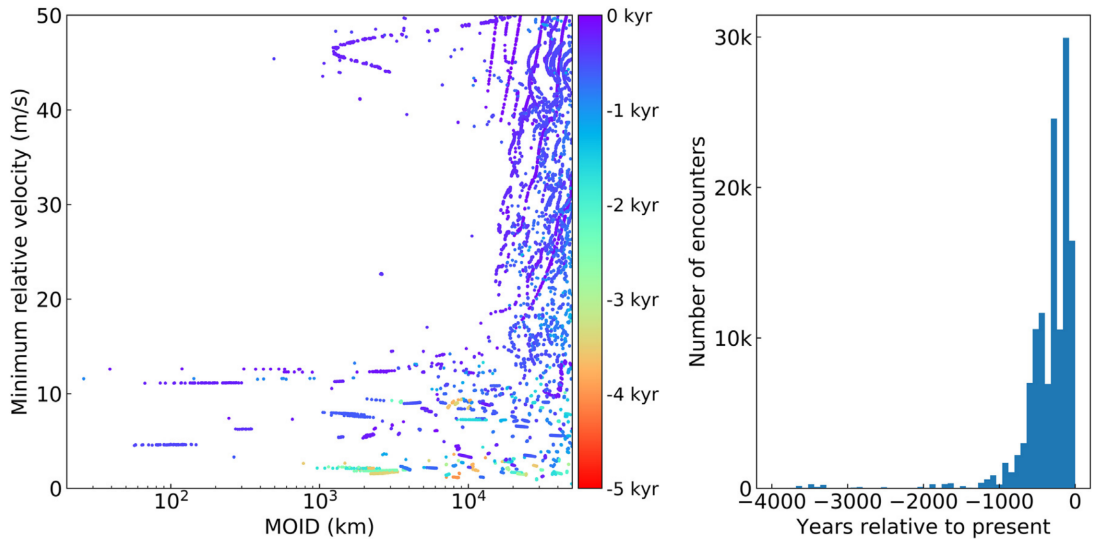

Figure 3.6: Left: The minimum relative velocity vs MOID during an encounter in the last 5 kyr for 2015 EE7 and 2015 FP124. The color of points indicates the time when the encounter happened. Right: Histogram of the recorded encounters from the left figure.

Table 3.5: Orbital elements at epoch 2458500.5 for the members of the two studied asteroid pairs with their absolute magnitudes from Lowell Observatory's `astorb` database.

Asteroid	H [mag]	a [AU]	e	i	Ω	ω	M
2015 EE7	20.2	1.702	0.411	27.31°	9.41°	219.2°	238.9°
2015 FP124	22.2	1.712	0.414	27.41°	9.41°	219.2°	236.3°
2017 SN16	23.2	1.016	0.016	13.38°	2.74°	137.0°	341.7°
2018 RY7	24.5	1.016	0.016	13.35°	2.82°	136.8°	344.3°

The calculated value of D for these two asteroids is only 0.0035, which indicates that these two orbits are extremely similar, see Table 3.5 for comparison of individual orbital elements. We did not record any close encounters to any of the mass objects in our integration in the past 10 kyr for any of orbital clones of the two asteroids, which makes the orbits evolution smooth and deterministic. With the help of several astrometric observations that we performed for both objects with SOAR and DCT[11] telescopes, observed arc extended to 391 days for 2017 SN16 and to 89 days for 2018 RY7. This resulted in orbital condition codes 1 and 4 for the primary and the secondary, respectively.

The results of our backward orbital integrations are clearer than in the case of 2015 EE7 and 2015 FP124 pair. In the right part of Figure 3.7 we see three clear spikes of time distribution of clone encounters at times around 7 700, 8 200 and 8 700 kyr ago. In the left part of the same figure we see that for encounters most distant from present ("oldest ones"), we recorded the slowest encounters with relative velocities as slow as 3 m/s and MOID on an orders ranging from 10^1 to 10^4 km. To better understand the distribution of clone encounters, we

[11]Discovery Channel Telescope (DCT) is a 4.3 meter telescope located in Arizona, USA.

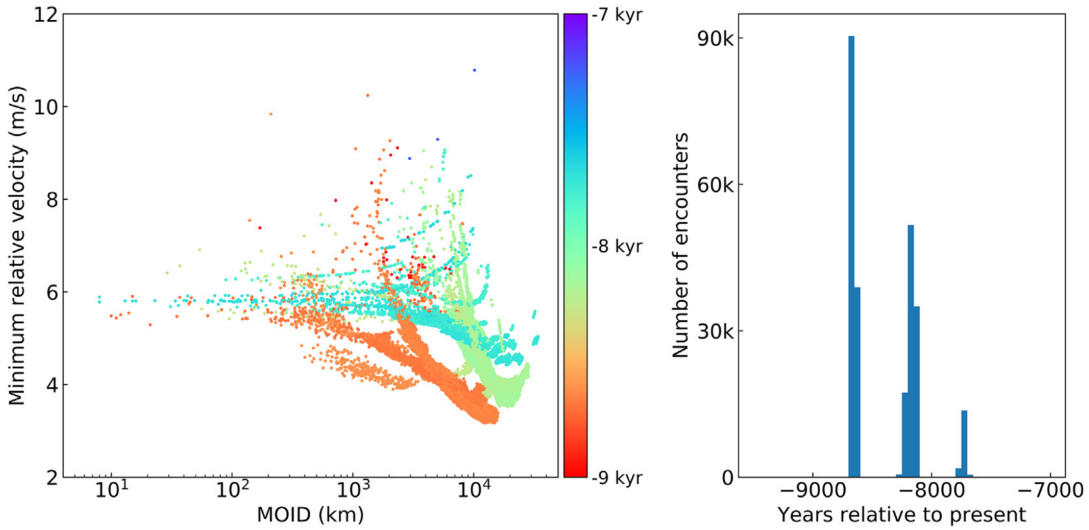

Figure 3.7: Left: The minimum relative velocity vs MOID during an encounter in the last 10 kyr for 2017 SN16 and 2018 RY7. The color of points indicates the time when the encounter happened. Right: Histogram of the recorded encounters from the left figure.

tracked the relative velocity and MOID evolution in time of the nominal orbits of 2017 SN16 and 2018 RY7 and 500 randomly selected clone pairs. In the left part of Figure 3.8 we see that the evolution of the relative velocity between clones has four minima, where the three "youngest" (closest to the present) correspond to the distribution peaks seen in Figure 3.7 right. They are caused by a secular variability with period $\sim$ 500 years. Because all the minima have very similar depth, different orbital clone pairs reach their minimum relative velocity in one of these minima. The leftmost minimum is cased due to outlying data points occurring in a single time-step and we do not see an association with low MOID values at these specific time steps and therefore, we did not consider them to be real encounters. From this results we were not able to determine the true separation event, but we were able to restrict the possible age, which happened somewhere between 7 500 and 9 000 kyr ago.

Both components of this probable asteroid pair were spectroscopically observed by Gemini South telescope. Even though the signal-to-noise ratio was small for both objects, especially for 2018 RY7, a taxonomic assignment was possible for both of them due to the deep absorption feature at 1µm. Both asteroids were classified as V-type asteroids (see Fig. 2 in Moskovitz et al., 2019). The observed fraction of near-Earth asteroids classified as V-types is 2-4% (Perna et al., 2018; Binzel et al., 2019; Devogèle et al., 2019) and the debiased fraction is below 1% (Stuart and Binzel, 2004). If we randomly select two asteroids from the near-Earth asteroid population, there is only a $\leq 0.2\%$ chance that we select two V-type asteroids. This makes these two asteroids a strong candidates of being genetically related.

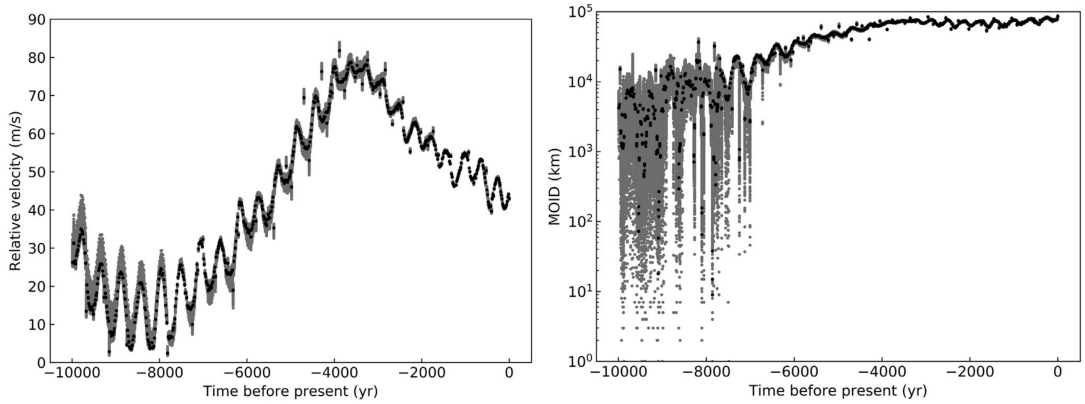

Figure 3.8: 2 Figures side by side

Summary

We have identified and further studied two candidate asteroid pairs among the near-Earth population. A common origin of both components of each pair is supported by their spectroscopic measurements, which resulted in the same taxonomic classification, S-complex for pair 2015 EE7–2015 FP124 and V-type for 2017 SN16–2018 RY7. This is a strong argument for pair 2017 SN16–2018 RY7, because the abundance of V-type asteroids in the near-Earth population is very low and the probability of randomly selecting two V-type asteroid from this population is very low. Since there is about 50% of S-complex asteroids (Perna et al., 2018; Binzel et al., 2019; Devogèle et al., 2019) (Stuart and Binzel, 2004, debiased estimation is 40%) this finding is not a strong argument for the hypothesis of a common origin, but it is still necessary to verify the taxonomy similarity of both pair components.

Age estimation of these pairs is a demanding task with a possible very useful outcome that can be used for testing a variety of models describing a rate of space weathering and spin state evolution. It was also confirmed that obtaining an accurate age estimation requires well constrained initial orbits. For the pair 2015 EE7–2015 FP124 we were only able to restrict the possible separation age to $< 5\,000$ kyr mainly due to the very short (13 days) observed arc for 2015 FP124. In the case of 2017 SN16–2018 RY7, we were able to restrict the time of a separation event that happened between 7500 and 9000 kyr ago, with times $\sim 7\,700$, $\sim 8\,200$ and $\sim 8\,700$ kyr ago being the most probable ones. Since the publication of this paper, new astrometrical observations were made for both these asteroids, which let to new condition codes 1 and 2 for 2017 SN16 and 2018 RY7, respectively (as of January 2020). We plan to rerun the backward orbital integration and use the new orbital solutions. We also plan to create larger number of orbital clones, shorten the time-step and most importantly, we will attempt to find physical, slow encounters between the orbital clones. In case of success, this would be a very strong argument that would even further support the hypothesis of a common origin of these two asteroids.

3.4 Cascade disruptions in asteroid clusters

In the paper Pravec et al. (2018) we came across a peculiar asteroid cluster of Emilkowalski. From the performed backward orbital integrations we did not get the same solution for its age among its members. We suggested that at least two separation events occurred in the recent history of this cluster and left a further study for future work. In Pravec et al. (2019) we found a new asteroid cluster as a by-product of our search for new asteroid pairs. Similarly as in the case of the cluster of Emilkowalki, the results of backward orbital integrations for this cluster, cluster of (157123) 2004 NW5, suggest two separation events significantly distant in time from each other. We decided to further explore this phenomenon and we searched for new asteroid clusters that would suggest at least two separation events. We found two additional such clusters, clusters of Kap'bos and (63440) 2001 MD30. We performed new detailed backward orbital integrations, with up-to-date orbit solutions, for all the four clusters. We also introduced a simple model that was used to test whether the YORP effect could be the cause of the fission events.

Search for cascade disruption candidates

To search for new asteroid clusters and new members of already known asteroid pairs and clusters, we used the catalog of osculating and mean orbital elements provided by `AstDyS-2` website. To quantify the similarity of two orbits, we used metric measuring distances in a five-dimensional space of orbital elements $d_{\mathrm{osc/mean}}$ described in Section 2. From experience we know that some asteroid clusters have "two cores" in the space of orbital elements, one of which is relatively close to the primary and the other can quite distant from it. This can be seen in Figure 3.9 in the d_{mean} distribution of the Emilkowalski cluster members, where three secondaries are distributed within $d_{\mathrm{mean}} \leq 22$ m/s while another three members are gathered at distances around 110 m/s. Therefore, we performed an extended search for new members of already known clusters published in Pravec et al. (2018). We tested the secular angle convergence (see description in Section 2.2.2) for all asteroids within the distance up to several hundreds m/s. In the densely populated regions around cluster primaries, we tested all asteroids with $d_{\mathrm{mean}} \leq 400$ m/s and for the least dense regions we tested all asteroids with $d_{\mathrm{mean}} \leq 750$ m/s. We typically obtained anywhere between 150 and 350 nearby asteroids, whose nominal orbits was integrated 5 Myr into the past and the convergence of secular angles with the orbital history of the primary was checked together with d_{osc} time evolution between given primary and given asteroids. Similar approach was taken for all asteroid pairs mentioned in Pravec et al. (2019), but used orbital catalogs did not grew much since its publication and we did not find any new clusters apart from the ones mentioned already in the paper. We also performed a search for new asteroid clusters by analysing the full catalog of mean orbital elements, but we did not find any additional clusters suggesting multiple ages.

Membership confirmation and age estimation

For the four clusters, all its confirmed members and all candidate members, we performed backward orbital integrations, in which we searched for close and slow encounters between individual secondaries and a given primary of a cluster. In two clusters, Emilkowalski and Kap'bos, we also searched for slow encounters between two selected secondaries to check the possibility of separation from each other rather both being separated from the primary. We created 1 000 orbital clones for each asteroid and assigned them with various possible strength of the Yarkovsky drift (for details see the last paragraph of Section 2.2 and references herein). We included the gravitational attraction of the Sun, the 8 major planets, two dwarf planets Pluto and Ceres and two large asteroids Vesta and Pallas. We used the symplectic integrator `WHFast` with a fixed time-step of 6 hours and we checked for slow encounters every 10 days.

We also performed a simple test whose goal was to estimate the minimum time required for a primary's and a secondary's secular angles to converge with the inclusion of Yarkovsky drift. We created three Yarkovsky clones of nominal orbits for all members of a given cluster and assigned them with zero, maximum positive and maximum negative Yarkovsky drift. Then we compared the secular angle evolution of the all nine clone combinations of a primary and each secondary of given cluster and we found the shortest time for the secular angles to converge. More detailed description of this method can be found in Section 2.2.1.

Two rotational fission induced via YORP effect

The formation mechanism of asteroid clusters with at least two generations of secondaries is still unknown and only a few hypotheses exist. We tested one hypothesis with following model. We assumed that the current primaries and their parent asteroids (before rotational fission) were shaped as prolate spheroids with semi-major axis a_p, b_p, c_p with $a_p \geq b_p = c_p$, where the c_p axis is also the rotational axis of the modeled asteroid. The equatorial elongations a_p/b_p of primaries were estimated from their observed lightcurve amplitudes A using the relation[12] $A = 2.5 \log a_p/b_p$. In our model, we started with an elongated asteroid with mass equal to the sum of masses of all known cluster members (before any separation events) with an assumed bulk density and geometric albedo for a given taxonomic type of the primary. We calculated its critical rotational frequency f_{crit} as

$$f_{\mathrm{crit}} = \sqrt{G\rho \left(e_{\mathrm{p}}^2 - 1\right) \left[2e_{\mathrm{p}} + \ln\left(\frac{1-e_{\mathrm{p}}}{1+e_{\mathrm{p}}}\right)\right] / \left(2\pi e_{\mathrm{p}}^3\right)}, \tag{3.7}$$

where $e_{\mathrm{p}} \equiv \sqrt{1 - b_{\mathrm{p}}^2/a_{\mathrm{p}}^2}$ (Richardson et al., 2005). Then, the asteroid was split up and one or more secondaries (first generation) escaped from the longest ends of the body at an escape velocity of the remaining primary body (intermediate parent). We assumed that the energy needed for all the secondaries to escape

[12] We note that this relation is derived for zero solar phase angle with an equator-on viewing aspect. In a general case these two conditions are not met. However, the non-zero solar phase angle increases an observed amplitude, whereas the tilted rotational axis decreases it. This means that these two effects work in opposite directions and we consider this equation to be a reasonable approximation for the asteroid equatorial elongation for our purpose.

was transferred from the rotation of the parent body and we calculated the new rotational frequency of the intermediate parent. Like in Pravec et al. (2008), we adjusted the strength of the YORP effect from Čapek and Vokrouhlický (2004) to match the physical parameters (size, bulk density, distance from the Sun) of our slowed down asteroid and we estimated the rotational acceleration $\dot{f}$ caused by the YORP effect. Then we simply calculated the time needed for the intermediate parent to reach f_{crit} again, so it could rotationally fission again and create a second generation of secondaries. We note that this model is simplified in several ways and its results should be treated as the first rough approximation, intended as a test whether the multi-fission disruption scenario induced only by the YORP effect is possible. We had to use several approximations and assumptions, because we lack detailed information about some of the physical parameters of the cluster members and their parents. For example, we assumed that the list of cluster members is complete, rotational energy of the secondaries is small and can be neglected, the shapes of the primary, the intermediate parent and the grand-parent asteroids are the same, only their sizes are different (for more see Section 4 in Fatka et al., 2020).

Results summary

At the time of writing this thesis, the paper Fatka et al. (2020) is still up-to-date a no additional findings have been made. In following sections is a brief summary of the results for each studied asteroid cluster. For more details we refer interested readers to the original paper in Attachments.

Cluster of (11842) Kap'bos

We found two new members of the Kap'bos cluster, asteroids (445874) 2012 TS255 and (439108) 2007 GD18, which are much more distant in the space of osculating or mean orbital elements ($d_{\mathrm{osc}} \sim 235$ m/s and $d_{\mathrm{mean}} \sim 260$ m/s) from the primary than the previously known two members ($d_{\mathrm{osc}} \leq 21$ m/s and $d_{\mathrm{mean}} \sim 1$ m/s). In fact, these two members are already mixed with a background asteroid population, see Figure 3.9. Based on the results of the clone encounters search, estimated nominal separation times for the "younger" two members, (228747) 2002 VH3 and (436415) 2011 AW46, are $\sim$ 465 and $\sim$ 230 kyr, respectively. Whereas for the "older" asteroids, the nominal separation times are $\sim$ 2 020 and $\sim$ 2 710 kyr for (445874) and (439108), respectively 3.6. The test of secular angle convergences with three Yarkovsky clones reviled that the nominal orbits of (445874) and (439108) require at least 1 000 and 1 100 kyr, respectively, to become coplanar with the orbit of the primary. Due to the great initial orbital similarity of (228747) and (436415) with the primary, we were not able to put any time restriction on them. We also found clone encounters between the two young secondaries (228747) and (436415) with hypothetical separation time $\sim$ 630 kyr ago. Our model predicted that after the first fission event and escape of (228747) and (436415), the remaining intermediate parent needs at least 2.16 Myr to reach its critical rotational frequency again.

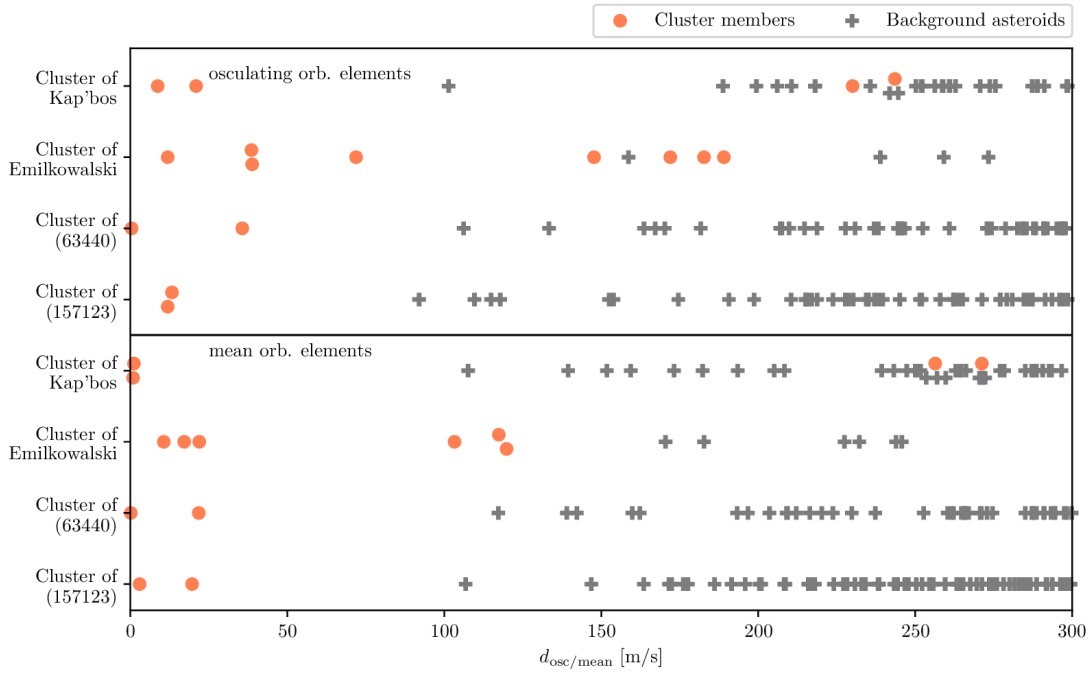

Figure 3.9: The distribution of distances of asteroids around the primaries of the four studied clusters in both osculating (top) and mean (bottom) orbital elements. Mean orbital elements are only available for multi-opposition asteroids. Small offsets along the y axis were applied to some points, where the cluster members' markers overlapped with other asteroid markers.

Cluster of (14627) Emilkowalski

We found a new probable member of the Emilkowalski cluster, a single-opposition asteroid 2018 VB69. With $d_{\mathrm{osc}} \approx 31$ m/s it is the second closest asteroid to the primary (in the space of osculating orbital elements). But because its observations span only across a single opposition, we did not verify its membership with orbital clone encounters method due to the initial large orbit uncertainty. With the backward orbital integrations, we verified the small age of secondaries (256124) 2006 UK337 and (224559) 2005 WU178, which is about 300 kyr. For the three "oldest" members (434002) 2000 SM320, 2014 UV143 and (476673) 2008 TN44, we obtained nominal ages $\sim$ 1 990, $\sim$ 2 470 and $\sim$ 3 020 kyr. For the last multi-opposition member of this cluster, (126761) 2002 DW10, we obtained an "in-between" age of $\sim$ 1 370 kyr. Our test with the Yarkovsky clones suggested that the "'young' members (256124) and (224559) need at least 200 kyr for their secular angles to converge with the primary. Whereas 900, 700 and 1 000 kyr is needed for the "older" members (434002), 2014 UV143 and (476673), respectively. No restriction could be put for (126761). After the first rotational fission and the escape of the "old" core (we also included asteroid (126761) in this group), the time required by YORP to spin-up the remaining intermediate parent to its critical rotational frequency is about 39 Myr, which substantially longer time than the one observed in out backward orbital integrations.

Cluster of (63440) 2001 MD30

Regarding the cluster of (63440) 2001 MD30, we verified the proposed membership (Pravec et al., 2019, by) of asteroid 2008 VS46 to this cluster, which now counts three members. The backward orbital integration suggest a separation time $\sim$ 70 kyr for the previously known member (331933) 2004 TV14 and $\sim$ 780 kyr for 2008 VS46. Asteroid (331933) is extremely close to the primary with $d_{\rm osc}$ = 0.4 m/s and $d_{\rm mean}$ = 0.1 m/s, therefore, the estimated young age is not surprising[13]. We were able to restrict the time needed for orbits of the primary and 2008 VS46 to become coplanar, which is at least 270 kyr ago, which is significantly longer time than the estimated separation time of (331933) from the primary. Due to the small size of the "older" secondary 2008 VS46, which separated first, the shortest time needed for the intermediate parent to undergo another rotational fission is only about 120 kyr.

Cluster of (157123) 2004 NW5

We did not find any new members of the cluster of (157123) 2004 NW5, therefore the count of its members remains at number three, as discovered by Pravec et al. (2019). We estimated the separation time $\sim$ 250 kyr for 2002 QM97 and $\sim$ 1 800 kyr for (385728) 2005 UG350. We estimated that the minimum time required for the orbits of the primary and (385728) to become coplanar is around 420 kyr, which is much shorter time than the nominal separation age obtained from the clone encounter method, but the requirement for orbital coplanarity is only a necessary condition and does not guarantee that other orbital elements are similar enough for an occurrence of slow encounters. We did not obtain an estimation of the time needed for the second rotational fission to happened, because there is not enough energy in the system for the "older" secondary to escape. The secondary (385728) holds about 1/4 of the mass of this cluster and a total of 166% of the rotational energy of the parent body rotating at $f_{\rm crit}$ is required.

Discussion

The hypothesis of two rotational fission induced only by a YORP spin-up seems plausible for the cluster of Kap'bos. From our model, the time necessary for an intermediate parent (parent after the escape of the two "older" secondaries) is about 2.16 Myr, which very close to the $\sim$ 2 Myr difference in separation times we got between the "young" and "old" groups of secondaries from our backward orbital integrations. If we also consider the uncertainties of the secondary age estimates, the assumed physical parameters and the simplicity of our model, the proposed hypothesis is consistent with our data for the Kap'bos cluster.

The cluster of Emilkowalski is a very interesting case. The results of our backward orbital integrations clearly indicated at least two separation events in the last 5 Myr. But our model predicted that the time required between the two disruption events is at least 38.7 Myr, assuming that both disruption events were rotational fission and YORP effect was responsible for the asteroid spin-up. It was evident that our model did not fit observed data and another process was involved

[13]For completeness, asteroid 2008 VS46 is located at distances $d_{\rm osc} \approx 36$ m/s and $d_{\rm mean} = 22$ m/s.

Table 3.6: Members of the asteroid cluster of (11842) Kap'bos with their absolute magnitudes H, distances $d_{\mathrm{osc/mean}}$ to the primary and estimated separation times T_{sep} in the past from the primary. In brackets is the ordinal number of given asteroid ordered by the distance from the primary in given orbital elements.

Asteroid		H [mag]	d_{osc} [m/s]	d_{mean} [m/s]	T_{sep} [kyr]
(11842)	Kap'bos	14.42 ± 0.03^a	-	-	-
(228747)	2002 VH3	17.16 ± 0.04^a	20.9 (2.)	1.1 (2.)	465^{+917}_{-308}
(445874)	2012 TS255	17.9	243.4 (13.)	271.2 (28.)	2017^{+1156}_{-623}
(349108)	2007 GD18	18.0	230.1 (10.)	256.4 (19.)	2708^{+656}_{-838}
(436415)	2011 AW46	18.3	8.7 (1.)	0.9 (1.)	226^{+679}_{-127}
(14627)	Emilkowalski	13.61 ± 0.06^a	-	-	-
(126761)	2002 DW10	15.3	71.9 (4.)	22.0 (3.)	1368^{+770}_{-414}
(256124)	2006 UK337	15.9	11.9 (1.)	17.2 (2.)	294^{+1452}_{-77}
(224559)	2005 WU178	16.6	38.8 (3.)	10.7 (1.)	311^{+1183}_{-86}
(434002)	2000 SM320	16.9	189.1 (9.)	119.8 (6.)	1991^{+724}_{-385}
	2014 UV143	17.5	147.7 (5.)	103.3 (4.)	2470^{+1500}_{-750}
	2009 VF107	17.6	172.0 (7.)	-	-
(476673)	2008 TN44	17.8	182.7 (8.)	117.4 (5.)	3020^{+1232}_{-1340}
	2018 VB69	18.0^b	30.9 (2.)	-	-
(63440)	2001 MD30	15.63 ± 0.13^a	-	-	-
(331933)	2004 TV14	17.4	0.4 (1.)	0.1 (1.)	68^{+151}_{-31}
	2008 VS46	19.2	35.7 (2.)	21.8 (2.)	778^{+112}_{-119}
(157123)	2004 NW5	16.93 ± 0.07^a	-	-	-
(385728)	2005 UG350	17.6	13.3 (2.)	19.7 (2.)	1792^{+922}_{-496}
	2002 QM97	18.6	11.9 (1.)	3.0 (1.)	248^{+397}_{-114}

[a] From Pravec et al. (2018).

[b] From `JPL Small-Body Database`. The remaining H values are taken from the `AstDyS-2` database.

in the formation of this cluster. Also the apparent association of the cluster with the observed dust band at $i \approx 17^\circ$ (see e.g. Vokrouhlický et al., 2008b; Espy Kehoe et al., 2015) and the rare D-type taxonomic classification (Vereš et al., 2015) of the primary are very interesting. We suspected that Emilkowalski might in fact be a cometary nucleus. More data, especially on the primary's shape, its bulk density and rotational axis orientation (of the primary as well the secondaries) would significantly advance our understanding of this cluster. We plan to confirm the D-type classification soon and further study this cluster.

For the cluster of (63440) we saw a significant gap between the estimated separation times for its two secondaries obtained from the results of clone encounters. The nominal separation times are about 700 kyr distant from each other, whereas the time required by YORP to spin-up the intermediate parent to its f_{crit} again is only about $120kyr$. This means that the formation mechanism of this cluster can be explained by two rotational fission events of the same asteroid and the YORP acceleration is sufficient. The large difference between necessary time required from our model and estimated separation times from integrations means that there could be another, yet undiscovered, cluster member that separated together with the older secondary. Or simply the parameters of the spin state were not optimal for the YORP effect to act at its maximum strength meaning smaller $\dot{f}$ and longer time between fission events.

Regarding the cluster (157123), from our integrations we saw a gap of ~ 1.5 Myr between the nominal separation times for the two secondaries. Due to the high mass ratio of the larger secondary (385728) and the parent body (~ 0.25), the escape of the secondary after rotational fission is formally not possible in our model. This could be due to an error in the estimated cluster parameters or maybe, we did not find the true primary of this cluster meaning that the (385728) did not separate from the (157123).

We also searched for common properties of the four clusters, but we did not find any obvious ones. These clusters have various number of members, they are located in different parts of the main belt and in total three different taxonomic types were assigned for the four primaries of the clusters.

Conclusion

In Pravec et al. (2018), we found three new asteroid clusters and several new members of already known clusters. By backward orbital integrations, we confirmed the membership of individual members, excluded potential interlopers and estimated the age of each cluster. The prediction of the proto-system separation model (originally derived for asteroid pairs) was generalized to account for N secondaries and 11 of the 13 studied clusters followed the same dependency of primary's rotational period on the mass ratio of the primary and all the secondaries. For the two outlying high-mass ratio clusters another formation mechanism (such as collision) was probably involved in their formation. It appears that asteroid clusters are similar to asteroid pairs meaning that both are formed by a rotational fission of a rubble pile asteroid, with the difference in the number of members. It is possible that in the future, new members will be found for many asteroid pairs making them asteroid clusters.

There are many interesting results in the paper by Pravec et al. (2019), we will try to point out the most interesting ones. We verified the shared origin of 93 asteroid pairs and estimated their age by (an improved version of) backward orbital integrations. We gathered enough photometrical data to derive the rotational periods of the 93 primaries and several secondaries. The vast majority (86) of the 93 pairs show the same correlation of the primary's rotational period and the mass ratio of the two component that is predicted by the proto-system separation model. For 19 asteroids from 17 pairs, we were able to determine the spin or orbit pole orientation. There is slightly more asteroids with a retrograde sense of rotation (10) than with prograde sense of rotation (7). In two cases we got poles orientation for the both components and, as expected, each of the two pairs have the same sense of rotation (both retrograde). For several asteroids with enough data, we were able to derive their convex model shape. A very interesting finding was that 13 primaries have at least one satellite orbiting around them and we presented two hypotheses of their formation. These pairs could be "failed asteroid clustrer" meaning that both secondaries were separated during a single fission event, but only one escaped from the system. Or the primary underwent two rotational fission (distant in time), the first resulted in a bound secondary, but after the second fission the system entered a chaotic stage of gravitational interaction of three bodies resulting in an escape of one of the secondaries.

In Moskovitz et al. (2019), we searched for asteroid pairs in the near-Earth population and we focused our subsequent study on two probable pairs. We adapted our backward orbital integration methods for the use in a more chaotic zone in the proximity to major planets. In our integrations, we found asteroid encounters with small MOID and low relative velocity, which support the hypothesis of a common origin and we were able to constrain the age for both pairs. Components of one pair were both taxonomically assigned V-type, which is very rare type in the near-Earth population and the probability of them also being on very similar orbits only by chance is extremely small. The components of the other pair were assigned a common S-complex. Currently, we are collecting more astrometrical data for some of these asteroids (and other candidates) and we plan to refine and extend the results of this work. The age estimation of these close

asteroid pairs is valuable for testing a variety of models including those related to space weathering and spin state evolution.

In Fatka et al. (2020), we searched for asteroid clusters indicating at least two, in time distinguishable, separation events. We found four such clusters, where one was pointed out in Pravec et al. (2018), one was a by-product from Pravec et al. (2019). For the remaining two clusters we found new members with a significantly different estimated separation times than the age estimated for the previously known members. We performed an extended search for new cluster members for the four clusters and verified their membership. We performed new backward orbital integrations for all members with a higher number of orbital clones and smaller time-step than we did before and we confirmed the previously estimated ages of given cluster members (if available). We created a simple model to test whether a hypothesis of two rotational fission evens caused by YORP is possible. We tested if the YORP effect is strong enough to spin-up the primary asteroid after the first fission so it can reach its critical rotation frequency again and undergo another fission in time. It turned out that this hypothesis is applicable for two of the four clusters. In one of the "failed" cases, the time required for a rotational fission was almost $20\times$ longer than what we see in our integrations and in the other case, there was not enough energy in the system to eject the larger secondary out of the system. It is interesting to see that the YORP effect is strong enough to keep spinning up asteroids and make them fission at least twice in a relatively short time scales. It is also interesting that there is probably another, yet unknown, mechanism responsible for the formation of some of the asteroid clusters. Finally, we looked for some common properties of the four cluster, but since we did not find any, it seems that cascade disruptions may occur in any asteroid cluster.

Bibliography

Bertotti, B., Farinella, P., and Vokrouhlický, D. (2003). *Physics of the Solar System - Dynamics and Evolution, Space Physics, and Spacetime Structure.*, volume 293.

Binzel, R. P., DeMeo, F. E., Turtelboom, E. V., Bus, S. J., Tokunaga, A., Burbine, T. H., Lantz, C., Polishook, D., Carry, B., Morbidelli, A., Birlan, M., Vernazza, P., Burt, B. J., Moskovitz, N., Slivan, S. M., Thomas, C. A., Rivkin, A. S., Hicks, M. D., Dunn, T., Reddy, V., Sanchez, J. A., Granvik, M., and Kohout, T. (2019). Compositional distributions and evolutionary processes for the near-Earth object population: Results from the MIT-Hawaii Near-Earth Object Spectroscopic Survey (MITHNEOS). *Icarus*, 324:41–76.

Bottke, William F., J., Vokrouhlický, D., Rubincam, D. P., and Nesvorný, D. (2006). The Yarkovsky and Yorp Effects: Implications for Asteroid Dynamics. *Annual Review of Earth and Planetary Sciences*, 34:157–191.

Bottke, W. F., Morbidelli, A., Jedicke, R., Petit, J.-M., Levison, H. F., Michel, P., and Metcalfe, T. S. (2002). Debiased Orbital and Absolute Magnitude Distribution of the Near-Earth Objects. *Icarus*, 156(2):399–433.

Bottke, W. F., Vokrouhlický, D., Walsh, K. J., Delbo, M., Michel, P., Lauretta, D. S., Campins, H., Connolly, H. C., Scheeres, D. J., and Chelsey, S. R. (2015). In search of the source of asteroid (101955) Bennu: Applications of the stochastic YORP model. *Icarus*, 247:191–217.

Breiter, S. and Michalska, H. (2008). YORP torque as the function of shape harmonics. *Mon. Not. Royal Astron. Soc.*, 388(2):927–944.

Breiter, S. and Vokrouhlický, D. (2011). Yarkovsky-O'Keefe-Radzievskii-Paddack effect with anisotropic radiation. *Mon. Not. Royal Astron. Soc.*, 410(4):2807–2816.

Burbine, T. H. (2016). Physical properties and families. In *Asteroids: Astronomical and Geological Bodies*, Cambridge Planetary Science, pages 185–217. Cambridge University Press.

Bus, S. J. (1999). *Compositional structure in the asteroid belt: Results of a spectroscopic survey*. PhD thesis, MASSACHUSETTS INSTITUTE OF TECHNOLOGY.

Carry, B. (2012). Density of asteroids. *Pla. Spa. Sci.*, 73(1):98–118.

Chesley, S. R., Farnocchia, D., Pravec, P., and Vokrouhlický, D. (2016). Direct Detections of the Yarkovsky Effect: Status and Outlook. In Chesley, S. R., Morbidelli, A., Jedicke, R., and Farnocchia, D., editors, *Asteroids: New Observations, New Models*, volume 318 of *IAU Symposium*, pages 250–258.

Chesley, S. R., Ostro, S. J., Vokrouhlický, D., Čapek, D., Giorgini, J. D., Nolan, M. C., Margot, J.-L., Hine, A. A., Benner, L. A. M., and Chamberlin, A. B.

(2003). Direct Detection of the Yarkovsky Effect by Radar Ranging to Asteroid 6489 Golevka. *Science*, 302(5651):1739–1742.

DeMeo, F. E., Alexander, C. M. O., Walsh, K. J., Chapman, C. R., and Binzel, R. P. (2015). The Compositional Structure of the Asteroid Belt. In *Asteroids IV*, pages 13–41.

DeMeo, F. E., Binzel, R. P., Slivan, S. M., and Bus, S. J. (2009). An extension of the Bus asteroid taxonomy into the near-infrared. *Icarus*, 202(1):160–180.

Devogèle, M., Moskovitz, N., Thirouin, A., Gustaffson, A., Magnuson, M., Thomas, C., Willman, M., Christensen, E., Person, M., Binzel, R., Polishook, D., DeMeo, F., Hinkle, M., Trilling, D., Mommert, M., Burt, B., and Skiff, B. (2019). Visible Spectroscopy from the Mission Accessible Near-Earth Object Survey (MANOS): Taxonomic Dependence on Asteroid Size. *Astron. J.*, 158(5):196.

Drummond, J. D. (1981). A test of comet and meteor shower associations. *Icarus*, 45(3):545–553.

Ďurech, J., Vokrouhlický, D., Kaasalainen, M., Higgins, D., Krugly, Y. N., Gaftonyuk, N. M., Shevchenko, V. G., Chiorny, V. G., Hamanowa, H., Hamanowa, H., Reddy, V., and Dyvig, R. R. (2008). Detection of the YORP effect in asteroid (1620) Geographos. *Astron. Astrophys.*, 489(2):L25–L28.

Espy Kehoe, A. J., Kehoe, T. J. J., Colwell, J. E., and Dermott, S. F. (2015). Signatures of Recent Asteroid Disruptions in the Formation and Evolution of Solar System Dust Bands. *Astrophys. J.*, 811(1):66.

Farinella, P., Vokrouhlický, D., and Hartmann, W. K. (1998). Meteorite Delivery via Yarkovsky Orbital Drift. *Icarus*, 132(2):378–387.

Farnocchia, D., Chesley, S. R., Vokrouhlický, D., Milani, A., Spoto, F., and Bottke, W. F. (2013). Near Earth Asteroids with measurable Yarkovsky effect. *Icarus*, 224(1):1–13.

Fatka, P., Pravec, P., and Vokrouhlický, D. (2020). Cascade disruptions in asteroid clusters. *Icarus*, 338:113554.

Harris, A. W. and Harris, A. W. (1997). On the Revision of Radiometric Albedos and Diameters of Asteroids. *Icarus*, 126(2):450–454.

Jacobson, S. A. and Scheeres, D. J. (2011). Dynamics of rotationally fissioned asteroids: Source of observed small asteroid systems. *Icarus*, 214(1):161–178.

Jedicke, R., Larsen, J., and Spahr, T. (2002). *Observational Selection Effects in Asteroid Surveys*, pages 71–87.

Kaasalainen, M., Ďurech, J., Warner, B. D., Krugly, Y. N., and Gaftonyuk, N. M. (2007). Acceleration of the rotation of asteroid 1862 Apollo by radiation torques. *Nature*, 446(7134):420–422.

Knežević, Z. (2017). Computation of Asteroid Proper Elements: Recent Advances. *Serbian Astronomical Journal*, 194:1–8.

Knežević, Z., Lemaître, A., and Milani, A. (2002). The Determination of Asteroid Proper Elements. In Bottke, W. F. J., Cellino, A., Paolicchi, P., and Binzel, R. P., editors, *Asteroids III*, pages 603–612.

Levison, H. F. and Duncan, M. J. (1994). The Long-Term Dynamical Behavior of Short-Period Comets. *Icarus*, 108(1):18–36.

Lowry, S. C., Fitzsimmons, A., Pravec, P., Vokrouhlický, D., Boehnhardt, H., Taylor, P. A., Margot, J.-L., Galád, A., Irwin, M., Irwin, J., and Kusnirák, P. (2007). Direct Detection of the Asteroidal YORP Effect. *Science*, 316(5822):272.

Milani, A. and Gronchi, G. F. (2010). *Theory of Orbital Determination*. Cambridge University Press.

Milani, A. and Knežević, Z. (1998). Asteroid Mean Elements: Higher Order and Iterative Theories. *Celestial Mechanics and Dynamical Astronomy*, 71(1):55–78.

Morbidelli, A., Bottke, W. F., J., Froeschlé, C., and Michel, P. (2002). Origin and Evolution of Near-Earth Objects. In *Asteroids III, W. F. Bottke Jr., A. Cellino, P. Paolicchi, and R. P. Binzel (eds), University of Arizona Press, Tucson, p.409-422*, pages 409–422.

Moskovitz, N. A., Fatka, P., Farnocchia, D., Devogèle, M., Polishook, D., Thomas, C. A., Mommert, M., Avner, L. D., Binzel, R. P., Burt, B., Christensen, E., DeMeo, F., Hinkle, M., Hora, J. L., Magnusson, M., Matson, R., Person, M., Skiff, B., Thirouin, A., Trilling, D., Wasserman, L. H., and Willman, M. (2019). A common origin for dynamically associated near-Earth asteroid pairs. *Icarus*, 333:165–176.

Nesvorný, D. and Vokrouhlický, D. (2006). New Candidates for Recent Asteroid Breakups. *Astron. J.*, 132(5):1950–1958.

Nesvorný, D. and Vokrouhlický, D. (2007). Analytic Theory of the YORP Effect for Near-Spherical Objects. *Astron. J.*, 134(5):1750.

Nesvorný, D. and Vokrouhlický, D. (2008). Analytic Theory for the Yarkovsky-O Effect on Obliquity. *Astron. J.*, 136(1):291–299.

Nesvorný, D., Vokrouhlický, D., and Bottke, W. F. (2006). The Breakup of a Main-Belt Asteroid 450 Thousand Years Ago. *Science*, 312:1490.

Novaković, B., Hsieh, H. H., and Cellino, A. (2012). P/2006 VW_{139}: a main-belt comet born in an asteroid collision? *Mon. Not. Royal Astron. Soc.*, 424(2):1432–1441.

Novaković, B., Hsieh, H. H., Cellino, A., Micheli, M., and Pedani, M. (2014). Discovery of a young asteroid cluster associated with P/2012 F5 (Gibbs). *Icarus*, 231:300–309.

Perna, D., Barucci, M. A., Fulchignoni, M., Popescu, M., Belskaya, I., Fornasier, S., Doressoundiram, A., Lantz, C., and Merlin, F. (2018). A spectroscopic survey of the small near-Earth asteroid population: Peculiar taxonomic distribution and phase reddening. *Pla. Spa. Sci.*, 157:82–95.

Piazzi, G. (1802). *Della scoperta del nuovo pianeta Cerere Ferdinandea, ottavo tra i primari del nostro sistema solare.*

Pravec, P., Fatka, P., Vokrouhlický, D., Scheeres, D. J., Kušnirák, P., Hornoch, K., Galád, A., Vraštil, J., Pray, D. P., Krugly, Y. N., Gaftonyuk, N. M., Inasaridze, R. Y., Ayvazian, V. R., Kvaratskhelia, O. I., Zhuzhunadze, V. T., Husárik, M., Cooney, W. R., Gross, J., Terrell, D., Világi, J., Kornoš, L., Gajdoš, Š., Burkhonov, O., Ehgamberdiev, S. A., Donchev, Z., Borisov, G., Bonev, T., Rumyantsev, V. V., and Molotov, I. E. (2018). Asteroid clusters similar to asteroid pairs. *Icarus*, 304:110–126.

Pravec, P., Fatka, P., Vokrouhlický, D., Scheirich, P., Ďurech, J., Scheeres, D. J., Kušnirák, P., Hornoch, K., Galád, A., Pray, D. P., Krugly, Y. N., Burkhonov, O., Ehgamberdiev, S. A., Pollock, J., Moskovitz, N., Thirouin, A., Ortiz, J. L., Morales, N., Husárik, M., Inasaridze, R. Y., Oey, J., Polishook, D., Hanuš, J., Kučáková, H., Vraštil, J., Világi, J., Gajdoš, Š., Kornoš, L., Vereš, P., Gaftonyuk, N. M., Hromakina, T., Sergeyev, A. V., Slyusarev, I. G., Ayvazian, V. R., Cooney, W. R., Gross, J., Terrell, D., Colas, F., Vachier, F., Slivan, S., Skiff, B., Marchis, F., Ergashev, K. E., Kim, D. H., Aznar, A., Serra-Ricart, M., Behrend, R., Roy, R., Manzini, F., and Molotov, I. E. (2019). Asteroid pairs: A complex picture. *Icarus*, 333:429–463.

Pravec, P., Harris, A. W., Kušnirák, P., Galád, A., and Hornoch, K. (2012). Absolute magnitudes of asteroids and a revision of asteroid albedo estimates from WISE thermal observations. *Icarus*, 221(1):365–387.

Pravec, P., Harris, A. W., and Michalowski, T. (2002). Asteroid Rotations. In *Asteroids III*, pages 113–122.

Pravec, P., Harris, A. W., Vokrouhlický, D., Warner, B. D., Kušnirák, P., Hornoch, K., Pray, D. P., Higgins, D., Oey, J., Galád, A., Gajdoš, Š., Kornoš, L., Világi, J., Husárik, M., Krugly, Y. N., Shevchenko, V., Chiorny, V., Gaftonyuk, N., Cooney, W. R., Gross, J., Terrell, D., Stephens, R. D., Dyvig, R., Reddy, V., Ries, J. G., Colas, F., Lecacheux, J., Durkee, R., Masi, G., Koff, R. A., and Goncalves, R. (2008). Spin rate distribution of small asteroids. *Icarus*, 197(2):497–504.

Pravec, P. and Vokrouhlický, D. (2009). Significance analysis of asteroid pairs. *Icarus*, 204(2):580–588.

Pravec, P., Vokrouhlický, D., Polishook, D., Scheeres, D. J., Harris, A. W., Galád, A., Vaduvescu, O., Pozo, F., Barr, A., Longa, P., Vachier, F., Colas, F., Pray, D. P., Pollock, J., Reichart, D., Ivarsen, K., Haislip, J., Lacluyze, A., Kušnirák, P., Henych, T., Marchis, F., Macomber, B., Jacobson, S. A., Krugly, Y. N., Sergeev, A. V., and Leroy, A. (2010). Formation of asteroid pairs by rotational fission. *Nature*, 466(7310):1085–1088.

Rein, H. and Liu, S. F. (2012). REBOUND: an open-source multi-purpose N-body code for collisional dynamics. *Astron. Astrophys.*, 537:A128.

Rein, H. and Spiegel, D. S. (2015). IAS15: a fast, adaptive, high-order integrator for gravitational dynamics, accurate to machine precision over a billion orbits. *Mon. Not. Royal Astron. Soc.*, 446(2):1424–1437.

Rein, H. and Tamayo, D. (2015). WHFAST: a fast and unbiased implementation of a symplectic Wisdom-Holman integrator for long-term gravitational simulations. *Mon. Not. Royal Astron. Soc.*, 452(1):376–388.

Richardson, D. C., Elankumaran, P., and Sand erson, R. E. (2005). Numerical experiments with rubble piles: equilibrium shapes and spins. *Icarus*, 173(2):349–361.

Richardson, D. C., Leinhardt, Z. M., Melosh, H. J., Bottke, W. F., J., and Asphaug, E. (2002). Gravitational Aggregates: Evidence and Evolution. In *Asteroids III*, pages 501–515.

Rosaev, A. and Plávalová, E. (2017). On the young family of 18777 Hobson. *Icarus*, 282:326–332.

Rubincam, D. P. (1995). Asteroid orbit evolution due to thermal drag. *J. Geophys. Res.*, 100(E1):1585–1594.

Rubincam, D. P. (1998). Yarkovsky thermal drag on small asteroids and Mars-Earth delivery. *J. Geophys. Res.*, 103(E1):1725–1732.

Scheeres, D. J. (2002). Stability in the Full Two-Body Problem. *Celestial Mechanics and Dynamical Astronomy*, 83(1):155–169.

Scheeres, D. J. (2007). Rotational fission of contact binary asteroids. *Icarus*, 189(2):370–385.

Scheeres, D. J. and Mirrahimi, S. (2008). Rotational dynamics of a solar system body under solar radiation torques. *Celestial Mechanics and Dynamical Astronomy*, 101(1-2):69–103.

Smirnov, E. A., Dovgalev, I. S., and Popova, E. A. (2018). Asteroids in three-body mean motion resonances with planets. *Icarus*, 304:24–30.

Southworth, R. B. and Hawkins, G. S. (1963). Statistics of meteor streams. *Smithsonian Contributions to Astrophysics*, 7:261–285.

Spoto, F., Milani, A., and Knežević, Z. (2015). Asteroid family ages. *Icarus*, 257:275–289.

Stuart, J. S. and Binzel, R. P. (2004). Bias-corrected population, size distribution, and impact hazard for the near-Earth objects. *Icarus*, 170(2):295–311.

Trilling, D., Mommert, M., Hora, J., Chesley, S., Emery, J., Fazio, G., Harris, A., Mueller, M., and Smith, H. (2016). NEOLegacy: The ultimate Spitzer survey of Near Earth Objects. Spitzer Proposal.

Usui, F., Kasuga, T., Hasegawa, S., Ishiguro, M., Kuroda, D., Müller, T. G., Ootsubo, T., and Matsuhara, H. (2013). Albedo Properties of Main Belt Asteroids Based on the All-Sky Survey of the Infrared Astronomical Satellite AKARI. *Astrophys. J.*, 762(1):56.

Čapek, D. and Vokrouhlický, D. (2004). The YORP effect with finite thermal conductivity. *Icarus*, 172(2):526–536.

Vereš, P., Jedicke, R., Fitzsimmons, A., Denneau, L., Granvik, M., Bolin, B., Chastel, S., Wainscoat, R. J., Burgett, W. S., Chambers, K. C., Flewelling, H., Kaiser, N., Magnier, E. A., Morgan, J. S., Price, P. A., Tonry, J. L., and Waters, C. (2015). Absolute magnitudes and slope parameters for 250,000 asteroids observed by Pan-STARRS PS1 - Preliminary results. *Icarus*, 261:34–47.

Vokrouhlicky, D. (1998). Diurnal Yarkovsky effect as a source of mobility of meter-sized asteroidal fragments. I. Linear theory. *Astron. Astrophys.*, 335:1093–1100.

Vokrouhlický, D. (1999). A complete linear model for the Yarkovsky thermal force on spherical asteroid fragments. *Astron. Astrophys.*, 344:362–366.

Vokrouhlický, D. and Bottke, W. F., J. (2001). The Yarkovsky thermal force on small asteroids and their fragments. Choosing the right albedo. *Astron. Astrophys.*, 371:350–353.

Vokrouhlický, D., Bottke, W. F., Chesley, S. R., Scheeres, D. J., and Statler, T. S. (2015). The Yarkovsky and YORP Effects. In Michel, P., DeMeo, F. E., and Bottke, W. F., editors, *Asteroids IV*, pages 509–531.

Vokrouhlický, D., Chesley, S. R., and Matson, R. D. (2008a). Orbital Identification for Asteroid 152563 (1992 Bf) Through the Yarkovsky Effect. *Astron. J.*, 135(6):2336–2340.

Vokrouhlický, D., Milani, A., and Chesley, S. R. (2000). Yarkovsky Effect on Small Near-Earth Asteroids: Mathematical Formulation and Examples. *Icarus*, 148(1):118–138.

Vokrouhlický, D. and Nesvorný, D. (2008). Pairs of Asteroids Probably of a Common Origin. *Astron. J.*, 136(1):280–290.

Vokrouhlický, D., Nesvorný, D., and Bottke, W. F. (2008b). Evolution of Dust Trails into Bands. *Astrophys. J.*, 672(1):696–712.

Vokrouhlický, D., Pravec, P., Durech, J., Bolin, B., Jedicke, R., Kušnirák, P., Galád, A., Hornoch, K., Kryszczyńska, A., Colas, F., Moskovitz, N., Thirouin, A., and Nesvorný, D. (2017). The young Datura asteroid family. Spins, shapes, and population estimate. *Astron. Astrophys.*, 598:A91.

Vokrouhlický, D., Ďurech, J., Pravec, P., Kušnirák, P., Hornoch, K., Vraštil, J., Krugly, Y. N., Inasaridze, R. Y., Ayvasian, V., Zhuzhunadze, V., Molotov, I. E., Pray, D., Husárik, M., Pollock, J. T., and Nesvorný, D. (2016). The Schulhof Family: Solving the Age Puzzle. *Astron. J.*, 151(3):56.

Žižka, J. and Vokrouhlický, D. (2011). Solar radiation pressure on (99942) Apophis. *Icarus*, 211(1):511–518.

Zappala, V., Cellino, A., Farinella, P., and Knezevic, Z. (1990). Asteroid Families. I. Identification by Hierarchical Clustering and Reliability Assessment. *Astron. J.*, 100:2030.

List of publications

In chronological order:

Asteroid clusters similar to asteroid pairs – Attachment A.1
Pravec P., Fatka P., Vokrouhlický D., Scheeres D., Kušnirák P., Hornoch K., Galád A. , Vraštil J., Pray D., Krugly Yu., Gaftonyuk N., Inasaridze R., Ayvazian V., Kvaratskhelia O., Zhuzhunadze V., Husárik M., Cooney W., Gross J., Terrell D., Világi J., Kornoš L., Š. Gajdoš, O. Burkhonov, Ehgamberdiev Sh., Donchev Z., Borisov G., Bonev T., Rumyantsev V., Molotov I.
Icarus 304:110–126 (2018)

Asteroid pairs: A complex picture – Attachment A.2
Pravec P., Fatka P., Vokrouhlický D., Scheirich P., Ďurech J., Scheeres D., Kušnirák P., Hornoch K., Galád A., Pray D., Krugly Yu., Burkhonov O., Ehgamberdiev Sh., Pollock J., Moskovitz N., Thirouin A., Ortiz J., Morales N., Husárik M., Inasaridze R., Oey J., Polishook D., Hanuš J., Kučáková H., Vraštil J., Világi J., Gajdoš Š., Kornoš L., Vereš P., Gaftonyuk N., Hromakina T., Sergeyev A., Slyusarev I., Ayvazian V., Cooney W., Gross J., Terrell D. , Colas F., Vachier F., Slivan S., Skiff B., Marchis F., Ergashev K., Kim D., Aznar A., Serra-Ricart M., Behrend R., Roy R., Manzini F., Molotov I.
Icarus 333:429–463 (2019)

A common origin for dynamically associated near-Earth asteroid pairs – Attachment A.3
Moskovitz N., Fatka P., Farnocchia D., Devogèle M., Polishook D., Thomas C., Mommert M., Avner L., Binzel R., Burt B., Christensen E., DeMeo F., Hinkle M., Hora J., Magnusson M., Matson R., Person M., Skiff B., Thirouin A., Trilling D., Wasserman L., Willman M.;
Icarus 333:165–176 (2019)

Cascade disruptions in asteroid clusters – Attachment A.4
Fatka P., Pravec P., Vokrouhlický D.
Icarus 338:113554 (2020)
DOI: https://doi.org/10.1016/j.icarus.2019.113554

A. Attachments

A.1 Asteroid clusters similar to asteroid pairs

A.2 Asteroid pairs: A complex picture

A.3 A common origin for dynamically associated near-Earth asteroid pairs

A.4 Cascade disruptions in asteroid clusters